



# Limitations of Emergent Constraints on Multi-Model Projections: Case Study of Constraining Vegetation Productivity With Observed Greening Sensitivity

Alexander J. Winkler<sup>1,2</sup>, Ranga B. Myneni<sup>3</sup>, and Victor Brovkin<sup>1</sup>

<sup>1</sup>Max Planck Institute for Meteorology, Bundesstrasse 53, 20146 Hamburg, Germany

<sup>2</sup>International Max Planck Research School on Earth System Modelling, Bundesstrasse 53, 20146 Hamburg, Germany

<sup>3</sup>Department of Earth and Environment, Boston University, Boston, Massachusetts 02215, USA

**Correspondence:** Alexander J. Winkler ([alexander.winkler@mpimet.mpg.de](mailto:alexander.winkler@mpimet.mpg.de))

## 1 Abstract.

2 Recent research on Emergent Constraints (EC) has delivered promising results. The method utilizes a measurable variable  
3 (predictor) from the recent historical past to obtain a constrained estimate of change in a difficult-to-measure variable (pre-  
4 dictand) at a potential future CO<sub>2</sub> concentration (forcing) from multi-model projections. This procedure critically depends  
5 on, first, accurate estimation of the predictor from observations and models, and second, on a robust relationship between  
6 inter-model variations in the predictor-predictand space. We investigate issues related to these two themes in this article, using  
7 vegetation greening sensitivity to CO<sub>2</sub> forcing during the satellite era as a predictor of change in Gross Primary Productivity  
8 (GPP) of the Northern High Latitudes region (60° N – 90° N, NHL) for a doubling of pre-industrial CO<sub>2</sub> concentration in the  
9 atmosphere. Greening sensitivity is defined as changes in annual maximum of green leaf area index (LAI<sub>max</sub>) per unit CO<sub>2</sub>  
10 forcing realized through its radiative and fertilization effects. We first address the question of how to realistically characterize  
11 the greening sensitivity of a large area, the NHL, from pixel-level LAI<sub>max</sub> data. This requires an investigation into uncertain-  
12 ties in LAI<sub>max</sub> data source and an evaluation of the spatial and temporal variability in greening sensitivity to forcing in both  
13 the data and model simulations. Second, the relationship between greening sensitivity and ΔGPP across the model ensemble  
14 depends on a strong coupling among simultaneous changes in GPP and LAI<sub>max</sub>. This coupling depends in a complex manner  
15 on the magnitude (level), time-rate of application (scenarios) and effects (radiative and/or fertilization) of CO<sub>2</sub> forcing. We  
16 investigate how each one of these three aspects of forcing can impair the EC estimate of the predictand (ΔGPP). Accounting  
17 for uncertainties in greening sensitivity and stability of the relation between inter-model variations results in a quantitative  
18 estimate of the uncertainty (± 0.2 Pg C yr<sup>-1</sup>) on constrained GPP enhancement (ΔGPP = +3.4 Pg C yr<sup>-1</sup>) for a doubling  
19 of pre-industrial atmospheric CO<sub>2</sub> concentration in NHL. This ΔGPP is 60% larger than the conventionally used average of  
20 model projections. The illustrated sources of uncertainty and limitations of the EC method go beyond carbon cycle research  
21 and are generally relevant for Earth system sciences.

22 *Copyright statement.*



## 1 1 Introduction

2 Earth system models (ESMs) are powerful tools to predict response to a variety of forcings such as increasing atmospheric  
3 concentration of greenhouse gases and other agents of radiative forcing (Klein and Hall, 2015). Still, longterm ESM projections  
4 of climate change can have substantial uncertainties. This can be due to poorly understood processes in some cases, and in  
5 others, to missing or simplified representations called parameterizations (Flato et al., 2013; Klein and Hall, 2015; Knutti et al.,  
6 2017). Certain important processes, especially in the atmosphere, happen at spatial scales finer than can be possibly represented  
7 in current ESMs. Consequently, certain key aspects of the system, such as variability, extreme precipitation events and large-  
8 scale climate modes, can be poorly simulated (Flato et al., 2013). Errors propagate and can be amplified through feedbacks  
9 among interacting components in the Earth system, resulting in biases whose origins can be difficult to identify (Flato et al.,  
10 2013). Furthermore, an inherent component of the Earth climatic system, its internal natural variability, is complicated to  
11 represent and simulate in models (Flato et al., 2013; Klein and Hall, 2015).

12 Model Intercomparison Projects aim is to explore these uncertainties by coordinating a wide range of simulation setups  
13 focusing on internal variability, boundary conditions, parameterizations, etc. (Taylor et al., 2012; Eyring et al., 2016; Flato  
14 et al., 2013; Knutti et al., 2017). Models developed at various institutions are driven with the same forcing information (e.g.  
15 historical forcing) or with identical idealized boundary conditions. However, each modeling group decides which of the pro-  
16 cesses to consider and implement in their ESM. The conventional approach of handling these multi-model ensembles is to use  
17 unweighted ensemble averages (Knutti, 2010; Knutti et al., 2017). This assumes that the models are independent of one another  
18 and equally good at simulating the climate system (Flato et al., 2013; Knutti et al., 2017). The large spread between model  
19 projections suggests that this assumption is not valid. Therefore, alternate methods have been developed to extract results more  
20 accurate than multi-model averages (e.g., model weighting scheme based on performance and interdependence, Knutti et al.,  
21 2017). The concept of *Emergent Constraints* arises in this context, namely, a method to reduce uncertainty in ESM projections  
22 relying on historical simulations and observations (Hall and Qu, 2006; Boé et al., 2009; Cox et al., 2013; Klein and Hall, 2015;  
23 Cox et al., 2018).

24 The two key parts of an Emergent Constraint (EC) based method are a linear relationship arising from the collective behavior  
25 of a multi-model ensemble and an observational estimate for imposing the said constraint (Fig. 1). The linear relationship is a  
26 physically (or physiologically) based correlation between inter-model variations in an observable entity of the contemporary  
27 climate system (*predictor*) and a projected variable (*predictand*) that is usually difficult to observe. Combining the emergent  
28 linear relationship with observations of the predictor sets a constraint on the predictand (Knutti et al., 2017; Klein and Hall,  
29 2015; Cox et al., 2013; Flato et al., 2013). Many such ECs have been identified and reported, as briefly summarized below.

30 Hall and Qu (2006) proposed a constraint on projections of snow-albedo feedback based on the correlation between large  
31 inter-model variations in feedback strength of the current seasonal cycle. The EC was first established for the CMIP3 ensemble  
32 and confirmed for phase five of the Coupled Model Intercomparison Project (CMIP5) (Qu and Hall, 2014; Flato et al., 2013).  
33 Several EC studies followed with the goal of reducing uncertainty in projections of the cloud feedback under global warming,  
34 as reviewed by Klein and Hall (2015). It is thought that erroneous representation of low-cloud feedback in ESMs contributes



1 essentially to the large uncertainty in equilibrium climate sensitivity (ECS, 1.5 to 5 K), i.e. warming for a doubling of pre-  
2 industrial atmospheric CO<sub>2</sub> concentration (2×CO<sub>2</sub>) (Klein and Hall, 2015; Sherwood et al., 2014). Recently, Cox et al. (2018)  
3 presented a different approach to constrain ECS based on its relationship to variability of global temperatures during the recent  
4 historical warming period. They report a constrained ECS estimate of 2.8 K for 2×CO<sub>2</sub> (66% confidence limits of 2.2 – 3.4  
5 K).

6 The concept of EC also found its way into the field of carbon cycle projections. A series of studies analyzed the extent  
7 to which inter-annual atmospheric CO<sub>2</sub> variability can serve as a predictor of longterm temperature sensitivity of terrestrial  
8 tropical carbon storage. Cox et al. (2013) and Wenzel et al. (2014) reported an emergent linear relationship, although with  
9 different slopes for CMIP3 and CMIP5 ensembles, resulting in slightly divergent constrained estimates (CMIP3:  $-53 \pm 17$   
10 Pg C K<sup>-1</sup>, CMIP5:  $-44 \pm 14$  Pg C K<sup>-1</sup>). Wang et al. (2014) however were unable to detect a similar relationship between  
11 the proposed predictor and predictand. Recently, Lian et al. (2018) presented an EC estimate of the global ratio of transpiration  
12 to total terrestrial evapotranspiration (T/ET), which is substantially higher ( $0.62 \pm 0.06$ ) than the unconstrained value ( $0.41 \pm$   
13  $0.11$ ). For the marine tropical carbon cycle, Kwiatkowski et al. (2017) identified an emergent relationship between the longterm  
14 sensitivity of tropical ocean net primary production (NPP) to rising sea surface temperature (SST) in the equatorial zone and  
15 the interannual sensitivity of NPP to El Niño/Southern Oscillation driven SST anomalies. Tropical NPP is projected to decrease  
16 by  $3 \pm 1\%$  for 1 K increase in equatorial SST according to the observational constraint.

17 Similar results were reported for extra-tropical terrestrial carbon fixation in a 2×CO<sub>2</sub> world. Plant productivity is expected  
18 to increase due to the fertilizing and radiative effects of rising atmospheric CO<sub>2</sub> concentration. Wenzel et al. (2016) focused  
19 on constraining the CO<sub>2</sub> fertilization effect on plant productivity in the northern high latitudes (60° N – 90° N, NHL) and  
20 the entire extra-tropical area in the northern hemisphere (30° N – 90° N) using the seasonal amplitude of longterm CO<sub>2</sub>  
21 measurements at different latitudes. They presented a linear relationship between the sensitivity of CO<sub>2</sub> amplitude to rising  
22 atmospheric CO<sub>2</sub> concentration and the relative increase in zonally averaged gross primary production (GPP) for 2×CO<sub>2</sub>. The  
23 observed CO<sub>2</sub> amplitude sensitivities at respective stations provided a constraint on the strength of the CO<sub>2</sub> fertilization effect,  
24 namely  $37\% \pm 9\%$  and  $32\% \pm 9\%$  for the NHL and the extra-tropical region, respectively.

25 Focusing on the NHL, Winkler et al. (2018) investigated how both effects of CO<sub>2</sub> enhance plant productivity while assess-  
26 ing the feasibility of vegetation greenness changes as a constraint (Fig. 1). Enhanced GPP due to the physiological effect and  
27 ensuing climate warming is indirectly evident in large-scale increase in summer time green leaf area (Myneni et al., 1997; Zhu  
28 et al., 2016). Historical CMIP5 simulations show that the maximum annual leaf area index (LAI<sub>max</sub>, leaf area per ground area)  
29 increases linearly with both CO<sub>2</sub> concentration and growing degree days (above 0°C, GDD0) in NHL. To avoid redundancy  
30 from co-linearity between the two driver variables, but retain their underlying time-trend and interannual variability, the dom-  
31 inant mode from a principal component analysis of CO<sub>2</sub> and GDD0 was used as the proxy driver (denoted  $\omega$ ). This greening  
32 sensitivity (i.e.  $\frac{\Delta \text{LAI}_{\text{max}}}{\Delta \omega}$ ) can be inferred for the overlapping historical period from simulations and observations alike. In all  
33 ESMs, changes in GPP arising from the combined radiative and physiological effects of CO<sub>2</sub> enrichment strongly correlate  
34 with changes in LAI<sub>max</sub> in the historical simulations. Thus, the large variation in modelled historical LAI<sub>max</sub> sensitivities lin-  
35 early maps to variation in  $\Delta \text{GPP}$  at 2×CO<sub>2</sub>. Hence, this linear relationship in inter-model variation between  $\Delta \text{GPP}$  at 2×CO<sub>2</sub>



1 and historical greening sensitivities allows using the observed sensitivity as an EC on  $\Delta\text{GPP}$  at  $2\times\text{CO}_2$  in NHL ( $3.4 \pm 0.2$   
2 Pg C yr<sup>-1</sup>, Winkler et al., 2018).

3 The EC method (Fig. 1) has its limitations. For example, Cox et al. (2013), Wang et al. (2014) and Wenzel et al. (2015)  
4 investigated on constraining future terrestrial tropical carbon storage using the same set of models and data. However, they  
5 arrived at different EC estimates and divergent conclusions. Some reasons for the failure and essential criteria required for  
6 successful application of the EC approach were described previously (Bracegirdle and Stephenson, 2012b; Klein and Hall,  
7 2015), but this list is far from complete. The main focus thus far has been on caveats establishing an emergent linear relationship  
8 in a multi-model ensemble. However, large uncertainty on the constraint could result potentially from how the observational  
9 predictor is derived and compared to the modeled estimates. Here, we revisit the study of Winkler et al. (2018) and elaborate  
10 on key issues concerning sources of uncertainty regarding the constraint and applicability of the EC method.

11 Uncertainty on the constrained estimate depends on (a) observed predictor and (b) modeled relationship, aside from the  
12 goodness-of-fit of the latter (green shading in Fig. 1). As for (a), the source of observations is an obvious first line of inquiry  
13 (Sect. 3.1). Spatial aggregation of data and model simulations introduces uncertainties, as the EC method is applied on large  
14 areal values of predictor and predictand. This is the subject of Sect. 3.2. The observed and modeled predictors are from the  
15 historical period. The representativeness, duration and match between data and models all introduce an uncertainty related  
16 to variations in the temporal domain – these are explored in (Sect. 3.3). The yellow shading in Fig. 1 represents the total  
17 uncertainty on observed predictor from these three fronts. Regarding (b), the modeled linear relation varies (grey shading in  
18 Fig. 1) depending on three attributes of the forcing, i.e. CO<sub>2</sub> concentration change, its magnitude, rate and effect (Sect. 3.4 and  
19 3.5). Lessons learned from analyses along these lines are presented in the conclusion section at the end.



## 1 2 Data and Methods

### 2 2.1 Observational data sets

#### 3 2.1.1 Remotely sensed leaf area index

4 We used the recently updated version (V1) of the leaf area index data set (LAI3g) developed by (Zhu et al., 2013). It was gen-  
5 erated using an artificial neural network (ANN) and the latest version (third generation) of the Global Inventory Modeling and  
6 Mapping Studies group (GIMMS) Advanced Very High Resolution Radiometer (AVHRR) normalized difference vegetation  
7 index (NDVI) data (NDVI3g). The latter have been corrected for sensor degradation, inter-sensor differences, cloud cover, ob-  
8 servational geometry effects due to satellite drift, Rayleigh scattering and stratospheric volcanic aerosols (Pinzon and Tucker,  
9 2014). This data set provides global and year-round LAI observations at 15-day (bi-monthly) temporal resolution and 1/12  
10 degree spatial resolution from July 1981 to December 2016. Currently, this is the only available record of such length.

11 The quality of previous version (V0) of LAI3g data set was evaluated through direct comparisons with ground measurements  
12 of LAI and indirectly with other satellite-data based LAI products, and also through statistical analysis with climatic variables,  
13 such as temperature and precipitation variability (Zhu et al., 2013). The LAI3gV0 data set (and related fraction vegetation-  
14 absorbed photosynthetically active radiation data set) has been widely used in various studies (Anav et al., 2013; Forkel et al.,  
15 2016; Zhu et al., 2016; Mao et al., 2016; Mahowald et al., 2016; Piao et al., 2014; Poulter et al., 2014; Keenan et al., 2016).  
16 The new version, LAI3gV1, used in our study is an update of that earlier version.

17 We also utilized a more reliable but shorter data set from the Moderate Resolution Imaging Spectroradiometer (MODIS)  
18 aboard the NASA's Terra satellite (Yan et al., 2016a, b). These data are well calibrated, cloud-screened and corrected for  
19 atmospheric effects, especially tropospheric aerosols. The sensor-platform is regularly adjusted to maintain a precise orbit. All  
20 algorithms, including the LAI algorithm, are physics-based, well-tested and currently producing sixth generation data sets.  
21 The data set provides global and year-round LAI observations at 16-day (bi-monthly) temporal resolution and  $0.05^\circ$  spatial  
22 resolution from 2000 to 2016.

23 Leaf area index is defined as the one-sided green leaf area per unit ground area in broadleaf canopies and as one-half the  
24 green needle surface area in needleleaf canopies in both observational and CMIP5 simulation data sets. It is expressed in units  
25 of  $\text{m}^2$  green leaf area per  $\text{m}^2$  ground area. Leaf area changes can be represented either by changes in annual maximum LAI  
26 ( $\text{LAI}_{\text{max}}$ ) (Cook and Pau, 2013), or growing season average LAI. In this study, we use the former because of its ease and  
27 unambiguity, as the latter requires quantifying the start- and end-dates of the growing season, something that is difficult to do  
28 accurately in NHL (Park et al., 2016) with the low resolution model data. Further,  $\text{LAI}_{\text{max}}$ , is less influenced by cloudiness and  
29 noise; accordingly, it is most useful in investigations of long-term greening and browning trends. The drawback of  $\text{LAI}_{\text{max}}$ , is  
30 the saturation effect at high LAI values (Myneni et al., 2002). However, this is less of a problem in high latitudinal ecosystems  
31 which are less-densely vegetated, with  $\text{LAI}_{\text{max}}$ , values typically in the range of 2 to 3.

32 The bi-monthly satellite data sets were merged to a monthly temporal resolution by averaging the two composites in the  
33 same month and bi-linearly remapped to the resolution of the applied reanalysis product ( $0.5^\circ \times 0.5^\circ$ , CRU TS4.01).



### 1 **2.1.2 Environmental driver variables**

2 We use temperature, precipitation and CO<sub>2</sub> data to derive the observed historical forcing (Sect. 2.3) and to calculate climatic  
3 regimes (Fig. 2). Monthly averages of near-surface air temperature and precipitation are from the latest version of the Cli-  
4 matic Research Unit Timeseries data set (CRU TS4.01). The global data are gridded to 0.5°×0.5° resolution (Harris et al.,  
5 2013). Global monthly means of atmospheric CO<sub>2</sub> concentration are from the GLOBALVIEW-CO<sub>2</sub> product (obspack\_co2\_1\_  
6 GLOBALVIEWplus\_v2.1\_2016\_09\_02; for details see <http://dx.doi.org/10.15138/G3259Z>) provided by the National Oceanic  
7 and Atmospheric Administration / Earth System Research Laboratory (NOAA / ESRL).

### 8 **2.2 Earth system model simulations**

9 We analyzed recent climate-carbon simulations of seven ESMs participating in the fifth phase of the Coupled Model Intercom-  
10 parison Project, CMIP (Taylor et al., 2012). The model simulated data were obtained from the Earth System Grid Federation,  
11 ESGF (<https://esgf-data.dkrz.de/projects/esgf-dkrz/>). Seven ESMs provide output for the variables of interest (GPP, CO<sub>2</sub>,  
12 LAI, and near-surface air temperature) for simulations titled esmHistorical, RCP4.5, RCP8.5, 1pctCO<sub>2</sub>, esmFixClim1, and  
13 esmFdbk1. It is the same set of models analyzed in Wenzel et al. (2016) and Winkler et al. (2018).

14 The esmHistorical simulation spanned the period 1850 to 2005 and was driven by observed conditions such as solar forcing,  
15 emissions or concentrations of short-lived species and natural and anthropogenic aerosols or their precursors, land use, anthro-  
16 pogenic as well as volcanic influences on atmospheric composition. The models are forced by prescribed anthropogenic CO<sub>2</sub>  
17 emissions, rather than atmospheric CO<sub>2</sub> concentrations.

18 Several Representative Concentration Pathways (RCPs) have been formulated describing different trajectories of greenhouse  
19 gas emissions, air pollutant production and land use changes for the 21st century. These scenarios have been designed based on  
20 projections of human population growth, technological advancement and societal responses (Vuuren et al., 2011; Taylor et al.,  
21 2012). We analyzed simulations forced with specified concentrations of a high emissions scenario (RCP8.5) and a medium  
22 mitigation scenario (RCP4.5) reaching a radiative forcing level of 8.5 and 4.5 W m<sup>-2</sup> at the end of the century, respectively.  
23 These simulations were initialized with the final state of the historical runs and spanned the period 2006 to 2100.

24 1pctCO<sub>2</sub> is an idealized fully coupled carbon-climate simulation initialized from a steady state of the preindustrial control  
25 run and atmospheric CO<sub>2</sub> concentration prescribed to increase 1% yr<sup>-1</sup> until quadrupling of the preindustrial level. The  
26 simulations esmFixClim and esmFdbk are set up similar to the 1pctCO<sub>2</sub> with the difference, that in esmFixClim (esmFdbk)  
27 only the radiative effect from increasing CO<sub>2</sub> concentration is included, while the carbon cycle sees the preindustrial CO<sub>2</sub>  
28 level (*vice versa*) (Taylor et al., 2009, 2012; Arora et al., 2013).

### 29 **2.3 Estimation of greening sensitivities**

30 We largely follow the methodology detailed in Winkler et al. (2018). For both model and observational data, the two-dimensional  
31 global fields of LAI and the driver variables are cropped according to different classification schemes (namely, vegetation  
32 classes (Olson et al., 2001), climatic regimes, and latitudinal bands). The aggregated values are area-weighted, averaged in



1 space, and temporally reduced to annual estimates dependent on the variable: annual maximum LAI, annual average atmo-  
2 spheric CO<sub>2</sub> concentration, and growing degree days (GDD0, yearly accumulated temperature of days where near-surface air  
3 temperature > 0° C).

4 We use a standard linear regression model to derive the greening sensitivity. On a global scale, LAI<sub>max</sub> is assumed to  
5 be a linear function of atmospheric CO<sub>2</sub> concentration. For the temperature-limited high northern latitudes, we also have to  
6 account for warming and include temperature as an additional driver. We do this using GDD0. We derive the dominant mode  
7 (denoted  $\omega$ ) through a principal component analysis of CO<sub>2</sub> and GDD0 to avoid redundancy from co-linearity between the  
8 two driver variables, but retain their underlying time-trend and interannual variability. Thus, NHL LAI<sub>max</sub> is formulated as a  
9 linear function of the proxy driver time series  $\omega$ . The best-fit gradients and associated standard errors of the linear regression  
10 model represent the LAI<sub>max</sub> sensitivities, or greening sensitivities, and their uncertainty estimates, respectively. For variations  
11 of finer spatial scale, the greening sensitivity is similarly calculated at the pixel scale.



### 1 3 Results and Discussion

2 There are two parts to the EC methodology (Fig. 1) – a statistically robust relationship between modeled matching pairs of  
3 predictor-predictand values and an observed value of the predictor. The predictors are from a representative historical period.  
4 The predictands are modeled changes in a variable of interest at a potential future state of the system, typically one that is diffi-  
5 cult to measure. The projection of the observed predictor on the modeled relation yields a constrained value of the predictand.  
6 A causal basis has to buttress the predictor-predictand relationship, else the EC method may be spurious. For example, mean-  
7 ingful coupling between concurrent changes in GPP and  $LAI_{max}$  with increasing atmospheric  $CO_2$  concentration underpins  
8 our specific case study, i.e. some of the enhanced GPP due to rising  $CO_2$  concentration is invested in additional green leaves  
9 by the plants (Winkler et al., 2018). This assures an approximately constant ratio of predictand to predictor across the models  
10 within the ensemble, thus setting up the potential for deriving an EC estimate.

11 Uncertainty on the constrained estimate depends on the observed predictor and modeled relationship, aside from the goodness-  
12 of-fit of the latter (Fig. 1). These are detailed below.

#### 13 3.1 Uncertainty in Observed Sensitivity Due to Data Source

14 We investigate this using LAI data from two different sources, AVHRR (1/12 degree) and MODIS (1/20 degree), and spatially  
15 aggregating these by broad vegetation classes, latitudinal bands and climatic regimes. The observed large-area sensitivities are  
16 always positive, irrespective of the source data and the method of aggregation (Fig. 2, Tab. 1). This indicates a net increase in  
17 green leaf area across the NHL during the observational period, as reported previously (Myneni et al., 1997; Zhu et al., 2016;  
18 Forkel et al., 2016). Overall, MODIS based estimates have higher uncertainty because of the shorter length of the data record  
19 (17 years). The failure to reliably estimate sensitivities in tropical forests (also in the latitudinal band  $30^\circ S - 30^\circ N$ , and in hot,  
20 wet and humid climatic regimes, see Tab. 1) is due to saturation of optical remote sensing data over dense vegetation ( $LAI_{max}$   
21  $> 5$ ) and problems associated with high aerosol content and ubiquitous cloudiness. In general, the estimated sensitivities are  
22 comparable across sensors and aggregation schemes (e.g. for latitudinal band  $> 60^\circ N/S$ , AVHRR:  $(3.4 \pm 0.5) \times 10^{-3}$ ;  
23 MODIS:  $(3.6 \pm 0.9) \times 10^{-3}$ ;  $LAI_{max}$   $ppm^{-1} CO_2$ ). However, there are three interesting exceptions. First, higher sensitivities  
24 are seen in croplands, which reflect management effects (fertilizer application, irrigation etc.) in addition to  $CO_2$  effects (Fig.  
25 2a, Tab. 1). Second, lower sensitivities are seen in sparsely vegetated areas and biomes (low  $LAI_{max}$ ,  $\sim 1$ ) which are due to  
26 nutritionally poor soils and / or inhospitable climatic conditions. Third, similarly low sensitivities are seen in dry regimes where  
27 precipitation is limiting and in humid regimes where temperature is limiting (Fig. 2c, Tab. 1).

28 This analysis illustrates the applicability and limitations of using observed greening sensitivities to  $CO_2$  forcing as a con-  
29 straint on photosynthetic production. For example, data from both AVHRR and MODIS sensors provide a comparable estimate  
30 of greening sensitivity in the colder high latitudes (boreal forests and tundra vegetation classes) where precipitation is generally  
31 less than 1000 mm (Winkler et al., 2018). However, the remote sensing LAI data are not suitable for similar studies in areas  
32 dominated by croplands and in the tropics for reasons stated above.





### 1 3.2 Uncertainty in Sensitivities Due to Spatial Aggregation

2 We focus further analyses on the NHL region ( $> 60^\circ$  N; Fig. 2b) only because data from both AVHRR and MODIS sensors yield  
3 comparable spatially-aggregated greening sensitivities in this region unlike elsewhere, as discussed in Sect. 3.1. In addition  
4 to the physiological effect of  $\text{CO}_2$ , also warming plays a key role in controlling plant productivity of these temperature-  
5 limited ecosystems, and thus, vegetation greenness. To avoid redundancy from co-linearity between  $\text{CO}_2$  and GDD0, we  
6 reduce dimensionality by performing a principal component analysis of the two driver variables (Sect. 2.3). The resulting first  
7 principal component explains most of the variance and retains the trend and year-to-year fluctuations in both  $\text{CO}_2$  and GDD0.  
8 Therefore, we obtain a proxy driver (hereafter denoted  $\omega$ ) that represents the overall forcing signal causing observed vegetation  
9 greenness changes in NHL. Accordingly, greening sensitivity for the entire NHL area is derived as response to  $\omega$ , the combined  
10 forcing signal of rising  $\text{CO}_2$  and warming. This procedure also enables a better comparability between observations and models  
11 because varying strengths of physiological and radiative effects of  $\text{CO}_2$  among models are taken into account (Sect. 3.3 – 3.5).

12 The vegetated landscape in the NHL region is heterogeneous, with boreal forests in the south, vast tundra grasslands to the  
13 north and shrublands in-between. The species within each of these broad vegetation classes respond differently to changes in  
14 key environmental factors. Even within a species, such responses might vary due to different boundary conditions, such as  
15 topography, soil fertility, micrometeorological conditions, etc. How this fine scale variation in greening sensitivity impacts the  
16 aggregated value is assessed below.

17 The distribution of greening sensitivities from all pixels is slightly skewed towards the positive (blue histogram). The mean  
18 value of this distribution (blue dashed line) is comparable to the sensitivity estimate derived from the spatially-averaged NHL  
19 time series (yellow dashed line; Fig. 3). Based on the Mann-Kendall test ( $p > 0.1$ ), nearly over half the pixels (54%) show pos-  
20 itive statistically significant trends (greening), while about 10% show browning trends (possibly due to disturbances, Goetz  
21 et al., 2005). The distribution of these statistically significant sensitivities (red histogram) therefore has two modes, a weak  
22 browning and a dominant greening mode, resulting in a substantially higher mean value (red dashed line) in comparison to the  
23 spatially-averaged estimate (yellow dashed line; Fig. 3). Thus, by taking into account the remaining 36% of non-significantly  
24 changing pixels (as in the NHL spatially-averaged estimate), an additional source of uncertainty is introduced. The mean sen-  
25 sitivity value is, of course, higher when only pixels showing a greening trend are considered in the analysis (green dashed line;  
26 Fig. 3). These are the only areas in NHL that actually show a large increase in plant productivity and consequently significant  
27 changes in leaf area. ESMs reveal similar pixel-level variation in both  $\text{LAI}_{\text{max}}$  sensitivity and associated changes in GPP in  
28 the NHL (Anav et al., 2013, 2015), although ESMs operate on much coarser resolution. Due to the coupling of the predictor  
29 and predictand, the distribution of all pixel estimates is approximately the same for the two variables. Accordingly, averaging  
30 the equally distributed estimates likely does not affect the predictor-predictand relationship in the model ensemble (Fig. 1).  
31 Consequently, if all spatial gridded data arrays are consistently processed to spatially-aggregated estimates, each predictand  
32 and predictor (observed and modeled) estimate contain a coherent  $\text{LAI}_{\text{max}}$  component of spatial variations. In other words, considering  
33 browning and non-significant pixels results in a lower overall  $\text{LAI}_{\text{max}}$  sensitivity in NHL, which in turn leads to a lower con-  
34 strained estimate of  $\Delta\text{GPP}$  in NHL. This is consistent with the underlying relationship between predictor and predictand. On a



1 related note, Bracegirdle and Stephenson (2012a) suggest that this source of error is not significantly dependent on the spatial  
2 resolution when comparing model subsets from high to low resolution.

3 The above analysis informs that spatially-averaged estimates are approximations containing a random error component  
4 due to inclusion of data from insignificantly changing pixels and a systematic bias component from browning pixels. This  
5 uncertainty is relevant to the EC method, where the observed sensitivity decisively determines the constrained estimate from  
6 the ensemble of ESM projections (Winkler et al., 2018; Kwiatkowski et al., 2017). However, if spatial variations are treated  
7 consistently as an inherent component of observations and models, the EC method is only slightly susceptible to this source of  
8 uncertainty.

### 9 **3.3 Uncertainty in Sensitivities Due to Temporal Variations**

10 We seek recourse to longterm CMIP5 ESM simulations covering the historical period 1850 to 2005 (Sect. 2.2) to assess  
11 temporal variation in the predictor variable, because of the shortness of observational record. Three representative models  
12 (CESM1-BGC, MIROC-ESM, and HadGEM2-ES) spanning a broad range of NHL greening sensitivity in the CMIP5 ensemble  
13 (Winkler et al., 2018) are selected for this analysis. For each model,  $LAI_{max}$  sensitivity to  $\omega$  in moving windows of different  
14 lengths (15, 30, and 45 years; Fig. 4) are evaluated. The analysis reveals two crucial aspects that highlight how temporal  
15 variations impair comparability of the predictor variable between models and observations – an essential component of the EC  
16 approach.

17 First, window locations of modeled and observed predictor variable have to match. If the forcing in the simulations is  
18 low, for example, as in the second half of the 19th century when  $CO_2$  concentration was increasing slowly, inter-annual  
19 variability dominates and  $LAI_{max}$  sensitivity cannot be accurately estimated irrespective of the window length (Fig. 4). With  
20 increasing forcing over time (rising yearly rate of  $CO_2$  infusion, and consequently, the concentration), the signal-to-noise  
21 ratio increases and  $LAI_{max}$  sensitivity to  $\omega$  estimation stabilizes, for example, as in the second half of the 20th century.  
22 Therefore,  $LAI_{max}$  sensitivities estimated at different temporal locations result in non-comparable values and eventually a  
23 false constrained estimate (details in Sect. 3.4). As an example, modeled sensitivities based on a 30-year window centered on  
24 year 1900, when  $CO_2$  level increased by 10 ppm, with observed sensitivity estimated from a 30-year window centered on year  
25 2000, when  $CO_2$  level increased by 55 ppm, describe different states of the system and therefore should not be used in the EC  
26 method.

27 Second, in addition to temporal location, window lengths have to match between observations and models. For all three  
28 models, sensitivities estimated from 15-year chunks show high variability and thus, a 15-year record is perhaps too short  
29 to obtain robust estimates. The  $LAI_{max}$  sensitivity estimation becomes more stable with strengthening forcing and increasing  
30 window length (Fig. 4). As a consequence, using short-term observed sensitivity as a constraint on long-term model projections  
31 results in an incorrect EC estimate. Hence, the MODIS sensor record is, on the one hand, too short and does not, on the other  
32 hand, overlap temporally with the historical CMIP5 forcing (Fig. 1). Therefore, it does not provide a correct observational  
33 constraint.



### 1 3.4 Level and Time Rate of CO<sub>2</sub> Forcing

2 The EC method raises an obvious question – does it not implicitly assume that the key operative mechanisms underpinning the  
3 EC relation remain unchanged because a future system state is being predicted based on its past behavior? To be specific, we  
4 are attempting to predict GPP at a future point in time based on greening sensitivity inferred from the past. Does this not require  
5 the assumption that the key underlying relationship which makes this prediction possible, namely, a robust coupling between  
6 contemporaneous changes in GPP and LAI<sub>max</sub> remains unchanged from the past to the future? To address this question, we  
7 resort to the CMIP5 idealized simulation (1pctCO<sub>2</sub>), where atmospheric CO<sub>2</sub> concentration increases 1% annually, starting  
8 from a preindustrial level of 284 ppm until a quadruple of this value is reached (Sect. 2.2). We limit the analysis to the three  
9 models (CESM1-BGC, MIROC-ESM, and HadGEM2-ES) which bracket the full range of GPP enhancement and LAI<sub>max</sub>  
10 sensitivity in the original seven ESM ensemble (Winkler et al., 2018).

11 The relationship between simultaneous changes in GPP and LAI<sub>max</sub> remains linear for all CMIP5 models in the range  
12 1×CO<sub>2</sub> to 2×CO<sub>2</sub> (Fig. 5, Tab. 2). With concentration increasing beyond 2×CO<sub>2</sub>, all models show weakening correlation  
13 ( $R^2$ , Tab. 2) and decreasing slope ( $b$ , Tab. 2) of this relationship (Fig. 5), suggesting a saturating rate of allocation of additional  
14 GPP to new leaves at higher levels of CO<sub>2</sub>. Consequently, LAI<sub>max</sub> sensitivity to increasing CO<sub>2</sub> and associated warming  
15 decreases. At and over 4×CO<sub>2</sub> (1140 ppm), a level unlikely to be seen in the near future, there appears to be no relationship  
16 between  $\Delta$ GPP and  $\Delta$ LAI<sub>max</sub>. This raises the question as to what extent does the weakening of relationship between the  
17 predictor and predictand (Fig. 1) at higher CO<sub>2</sub> concentration affects the EC analysis. To shed light on this matter, we perform  
18 the following *Gedankenexperiment*.

19 Understanding the relationship and interplay between forcing (increasing CO<sub>2</sub> concentration), predictor (LAI<sub>max</sub> sensitiv-  
20 ity), and the predictand ( $\Delta$ GPP) is key to evaluating the EC method. We conceive four possible scenarios of how the system  
21 might behave with increasing forcing. For simplicity, we assume linearly increasing CO<sub>2</sub> concentration, use LAI instead of  
22 LAI<sub>max</sub>, and GPP refers to its annual value below (Fig. 6). The four scenarios are: *All linear*, *all non-linear* (saturation), and  
23 two *mixed linear / non-linear* cases (Tab. A1). We emulate a multi-model ensemble by applying different random parame-  
24 terizations for the linear and saturation (the hyperbolic tangent function) responses. One of these realizations is assumed to  
25 represent pseudo-observations (dashed lines, Fig. 5). We discuss one case in detail for illustrative purposes (No. 3, Tab. A1).

26 In scenario 3,  $\Delta$ GPP increases linearly with increasing CO<sub>2</sub> (Fig. 6a), while  $\Delta$ LAI/ $\Delta$ GPP saturates (Fig. 6b). The LAI  
27 sensitivity to CO<sub>2</sub> weakens with increasing forcing (Fig. 6c) as a response to saturation of GPP allocation to leaf area. We  
28 derive LAI sensitivities to CO<sub>2</sub> for three different periods ('past periods' in Fig. 6c) to constrain  $\Delta$ GPP at a much higher  
29 CO<sub>2</sub> level ('projected period' in Fig. 6a). Next, we apply the EC method on these pseudo-projections of  $\Delta$ GPP relying on  
30 LAI sensitivities derived from the three past periods (Fig. 6d). The EC method is applicable even at a low forcing level (past  
31 period 1) in this simplified scenario because we neglect stochastic internal variability of the system. The slope of emergent  
32 linear relationship increases (Fig. 6d) as modeled LAI sensitivities decrease with rising CO<sub>2</sub> concentration (Fig. 6c). The  
33 observational constraint on future  $\Delta$ GPP, however, remains nearly the same, because pseudo-observed LAI sensitivity also  
34 weakens at higher CO<sub>2</sub> levels (dashed lines, Fig. 6c, d). Thus, the three EC estimates of  $\Delta$ GPP are approximately identical



1 (Fig. 6d) and independent of the forcing level during past periods. With intensified forcing, the relationship between predictor  
2 and predictand remains linear within the model ensemble, although their relationship becomes non-linear within each model  
3 and, crucially, in reality as well. In other words, as long as the models agree on the occurrence and "timing" of saturation,  
4 changes in predictor and predictand relate linearly within the model ensemble. The same behavior is also seen in the other  
5 three scenarios (Tab. A1; Fig. A1, A2).

6 Nevertheless, with ever increasing forcing and associated steepening of the emergent linear relationship, the LAI sensitivity  
7 loses its explanatory power at some point because the linear relationship eventually lies within the observational uncertainty  
8 and no meaningful constraint can be derived. This and disagreement between models on system dynamics are ultimate limits  
9 of the EC method. Interestingly, we find that all CMIP5 models agree on saturation, but slightly disagree on the timing of  
10 saturation. Further, we find that the 'all non-linear' scenario best describes the dynamics of the system in the forcing range  
11 from  $1\times\text{CO}_2$  to  $4\times\text{CO}_2$ . However, the saturation of LAI to GPP happens at a lower  $\text{CO}_2$  level than saturation of GPP to  $\text{CO}_2$   
12 (Fig. A2). Still, inferences from interpretation of Case 3 (Fig. 6) are equally applicable.

13 Results from the above *Gedankenexperiment* also highlight the importance of matching window locations and lengths be-  
14 tween models and observations, as discussed earlier (Sect. 3.3). For instance, taking LAI sensitivity from past period 2 (green  
15 dashed line, Fig. 6d) as an observational constraint on the multi-model linear relationship based on past period 3 (red solid line,  
16 Fig. 6d), results in a significant overestimation of constrained  $\Delta\text{GPP}$  (intersection of the two lines, Fig. 6d).

17 The above analysis informs that the constrained GPP estimate at one future period is nearly independent of the past periods  
18 from when the observational sensitivities are derived, for most realistic scenarios. Now, we evaluate the EC method where  
19 sensitivity from one past period is used to obtain constrained GPP estimates at different periods in the future, i.e. progressively  
20 farther down the time-line. We utilize the greening sensitivity derived from observed  $\text{LAI}_{\text{max}}$  data and apply the EC method to  
21 CMIP5 1pct $\text{CO}_2$  simulations. The sensitivities in this case are due to forcing from both  $\text{CO}_2$  increase and associated warming  
22 during the observational period (Sect. 2.3). We seek constrained GPP estimates at future  $\text{CO}_2$  levels ( $2\times\text{CO}_2$ ,  $3\times\text{CO}_2$ , and  
23  $4\times\text{CO}_2$ ).

24 Winkler et al. (2018) previously reported a strong linear relationship between modeled contemporaneous changes in  $\text{LAI}_{\text{max}}$   
25 and GPP arising from the combined radiative and physiological effects of  $\text{CO}_2$  enrichment until  $2\times\text{CO}_2$  in the CMIP5 ensem-  
26 ble (Fig. 5). As a result, models with low  $\text{LAI}_{\text{max}}$  sensitivity project lower  $\Delta\text{GPP}$  for a given increment of  $\text{CO}_2$  concentration,  
27 and *vice versa*. Thus, the large variation in modeled historical  $\text{LAI}_{\text{max}}$  sensitivities linearly maps to variation in  $\Delta\text{GPP}$  at  
28  $2\times\text{CO}_2$  (Winkler et al., 2018; blue line, Fig. 7a). At higher levels, such as  $3\times\text{CO}_2$  (green line,  $R^2 = 0.93$ ) and  $4\times\text{CO}_2$  (red  
29 line,  $R^2 = 0.88$ ), this linear relationship within the model ensemble, while still present, weakens (Fig. 7a; Tab. 3). This is  
30 because the CMIP5 models do not agree on the timing and magnitude of the saturation effect at higher  $\text{CO}_2$  levels (Fig. 7a).  
31 The increment in constrained GPP estimates for successive equal increments of  $\text{CO}_2$  decreases due to the saturation effect in  
32 all CMIP5 models (dashed horizontal lines, Fig. 7a). For example, the change in GPP between  $3\times\text{CO}_2$  and  $4\times\text{CO}_2$  ( $\Delta\text{GPP}$   
33  $\sim 1.06 \text{ Pg C yr}^{-1}$ , Tab. 3) is much lower than between  $2\times\text{CO}_2$  and  $3\times\text{CO}_2$  ( $\Delta\text{GPP} \sim 2.34 \text{ Pg C yr}^{-1}$ , Tab. 3).

34 We have thus far focused on the magnitude of  $\text{CO}_2$  concentration change and not on the time rate of this change. For  
35 example, a given amount of change in  $\text{CO}_2$  concentration, say 200 ppm, can be realized over different time periods, say over



1 a 100 or 150 years. The problem of varying rates of CO<sub>2</sub> concentration change is implicitly encountered when ESMs are  
2 executed under different forcing scenarios, such as RCPs. A question then arises whether the constrained GPP estimate is  
3 independent of the time rate of CO<sub>2</sub> concentration change and dependent only on the magnitude of CO<sub>2</sub> concentration change.  
4 To investigate this aspect of forcing, we extract GPP estimates at the same CO<sub>2</sub> concentration (535 ppm; final concentration  
5 in RCP4.5) from three simulations of different forcing rates and calculate the difference relative to a common initial CO<sub>2</sub>  
6 concentration (380 ppm; initial concentration of RCP scenarios). Hence, the magnitude of the forcing is the same but applied  
7 over different durations (RCP4.5: ~90yr, RCP8.5: ~45yr, and 1pctCO<sub>2</sub>: ~30yr). A clear majority of the CMIP5 models show  
8 substantial differences in ΔGPP between the different pathways of CO<sub>2</sub> forcing. In general, GPP changes are higher for lower  
9 time rates of CO<sub>2</sub> forcing, i.e. forcing over longer time periods. As a consequence, the EC estimates of ΔGPP for the same  
10 increase in CO<sub>2</sub> concentration are scenario-dependent (Fig. 7b; Tab. 3) – a counter-intuitive result. For instance, ΔGPP in the  
11 low-CO<sub>2</sub>-rate scenario (RCP4.5: ΔGPP ~2.84 Pg C yr<sup>-1</sup>, Tab. 3) is ~39% (1pctCO<sub>2</sub>: ΔGPP ~2.05 Pg C yr<sup>-1</sup>, Tab. 3) and  
12 ~20% (RCP8.5: ΔGPP ~2.38 Pg C yr<sup>-1</sup>, Tab. 3) higher than the high-CO<sub>2</sub>-rate scenarios for an increase of 155 ppm CO<sub>2</sub>.  
13 This analysis suggests that the vegetation response to rising CO<sub>2</sub> is pathway dependent, at least in the NHL. One of the reasons  
14 for this could be species compositional changes in scenarios of low forcing rates, i.e. over longer time frames. This novel result,  
15 however, requires a separate in-depth study.

### 16 3.5 Effects of CO<sub>2</sub> Forcing

17 Higher concentration of CO<sub>2</sub> in the atmosphere stimulates plant productivity through the fertilization and radiative effects  
18 (Nemani et al., 2003; Leakey et al., 2009; Arora et al., 2011; Goll et al., 2017). The two effects can be disentangled in  
19 the model world by conducting simulations in a 'CO<sub>2</sub> fertilization effect only' (esmFixClim1) and a 'radiative effect only'  
20 (esmFdbk1) setup (Sect. 2.2). These are termed below as idealized model simulations. We investigate here whether historical  
21 runs and observations, which include both effects, can be used to constrain GPP changes in idealized CMIP5 simulations (e.g.  
22 as in Wenzel et al. (2016)).

23 We find strong linear relationships between historical LAI<sub>max</sub> sensitivity and ΔGPP for 2×CO<sub>2</sub> in both idealized setups  
24 (esmFixClim1:  $R^2 = 0.92$ , esmFdbk1:  $R^2 = 0.98$ , Tab. 3, Fig. 7c). Consequently, this linear relationship is also pronounced for  
25 calculated sums of both effects for each model (esmFixClim1 + esmFdbk1:  $R^2 = 0.95$ , Tab. 3, Fig. 7c). This suggests that the  
26 two effects act additively on plant productivity and, thus, each effect can be simply expressed in terms of a scaling factor of  
27 the total GPP enhancement. Hence, the application of the EC method on idealized simulations using real world observations is  
28 conceptually feasible.

29 Interestingly, the two effects contribute about the same to the general increase in GPP at 2×CO<sub>2</sub> (esmFixClim1: ΔGPP  
30 ~1.35 Pg C yr<sup>-1</sup>, esmFdbk1: ΔGPP ~1.38 Pg C yr<sup>-1</sup>, Tab. 3, Fig. 7c). At higher concentrations, such as 3×CO<sub>2</sub> and  
31 4×CO<sub>2</sub>, the enhancement in GPP saturates in both idealized setups. However, the radiative effect becomes dominant relative to  
32 the CO<sub>2</sub> fertilization effect when CO<sub>2</sub> concentration exceeds 2×CO<sub>2</sub> (e.g. at 4×CO<sub>2</sub> esmFixClim1: ΔGPP ~2.42 Pg C yr<sup>-1</sup>,  
33 esmFdbk1: ΔGPP ~3.06 Pg C yr<sup>-1</sup>, Tab. 3). Therefore, we can expect that at some point in the future, NHL photosynthetic  
34 carbon fixation will benefit more from climate change (e.g. warming) than from the fertilizing effect of CO<sub>2</sub>.



### 1 3.6 Uncertainties in the multi-model ensemble

2 Besides methodological sources of uncertainty discussed above, the estimate of an EC may also be deficient due to inaccurate  
3 assumptions about the model ensemble. First, possible common systematic errors in a multi-model ensemble (i.e. the entire  
4 ensemble misses an unknown but for the future essential process) are implicitly omitted in the EC approach, however, could  
5 cause a general over- or underestimation of the constrained value (Bracegirdle and Stephenson, 2012b; Stephenson et al., 2012).  
6 Second, the set of forcing variables for historical simulations may be incomplete (i.e. not yet identified drivers of observed  
7 changes) and, thus, the comparability of observations and model simulations is limited (Flato et al., 2013). Third, the EC method  
8 can be overly sensitive to individual models of the ensemble, which has a bearing on the robustness of the constrained value  
9 (Bracegirdle and Stephenson, 2012b). Bracegirdle and Stephenson (2012b) proposed a diagnostic metric (Cook's distance)  
10 to test an ensemble for influential models. Fourth, the assumption behind the predictand-predictor relationship has to rely  
11 on a logical connection within the model ensemble, meaning that the analyzed characteristic of the predictor variable (e.g.  
12 sensitivity to the forcing, or historical relative/absolute changes) is causally linked to changes in the predictand variable. For  
13 instance, Wenzel et al. (2016) reported a linear relationship between relative changes in GPP for doubling of CO<sub>2</sub>, so changes  
14 relative to the preindustrial state, and historical sensitivity of CO<sub>2</sub> amplitude to rising CO<sub>2</sub>, so neglecting the initial state. This  
15 statistical relationship can be spurious, because the model skill of simulating an accurate initial state and a plausible sensitivity  
16 to a forcing are not connected.

17 These issues are to be contemplated when establishing an EC estimate and evaluating its robustness.



## 1 4 Conclusions

2 An in-depth analysis of the EC method is illustrated in this article through its application to projections of change in NHL  
3 photosynthesis under conditions of rising atmospheric CO<sub>2</sub> concentration. Key conclusions highlighting the functionality of  
4 the EC method are presented below.

5 The importance of how the observational predictor is obtained cannot be emphasized enough because it essentially defines  
6 the constrained estimate. Thus, considerable care is required when selecting and processing the observational datasets. The  
7 LAI data products of both AVHRR and MODIS sensors provide comparable estimates of greening sensitivity in the colder  
8 northern high latitudes (i.e. boreal forests and tundra vegetation classes). In these ecosystems, factors associated with GPP  
9 enhancement from CO<sub>2</sub> forcing and consequent investment in leaf area dominate. This is not the case in croplands and tropical  
10 areas. Therefore, the use of greening sensitivity as an observational constraint is not feasible in regions where croplands and/or  
11 tropical vegetation dominate.

12 Spatially aggregating observations and model output of different resolutions in the EC method is another source of un-  
13 certainty. Regional estimates of greening sensitivity are approximations of complex fine-scale processes. Aggregation will  
14 inevitably introduce a random error component due to inclusion of data from areas where LAI is not changing and a system-  
15 atic bias from areas where LAI is decreasing (browning). The spatially-aggregated greening sensitivity is meaningful only if  
16 most of the region is greening in response to CO<sub>2</sub> forcing. However, as long as spatial variations in observations and models  
17 simulations are treated consistently, this source of uncertainty is likely of minor importance.

18 A large source of uncertainty is associated with temporal variability of the predictor variable throughout the historical period.  
19 The evaluation of greening sensitivity requires temporal window lengths of sufficient duration, approximately 30 years, and  
20 location along the forcing time line. And, these should match between models and observations. For example, the analysis  
21 in Wenzel et al. (2016) might have yielded different results and conclusions if model and observational predictor sensitivities  
22 were temporally matched. The relevance of window length decreases with increasing and accelerating forcing, depending on  
23 the magnitude of natural/internal variability (signal-to-noise ratio) of the predictor variable.

24 The level, effect and duration of CO<sub>2</sub> forcing have a bearing on the linear relationship between GPP enhancement and  
25 predictor sensitivities (Fig. 1). For example, the relationship underpinning the EC method, namely, that between concurrent  
26  $\Delta\text{GPP}$  and  $\Delta\text{LAI}_{\text{max}}$ , changes with increasing forcing level (CO<sub>2</sub> concentration). This relation breaks down at very high  
27 CO<sub>2</sub> concentrations at which point the EC method fails. The two dominant effects of rising CO<sub>2</sub> concentration on vegetation,  
28 namely, the fertilization and radiative effects, appear to be approximately additive in terms of GPP enhancement to CO<sub>2</sub>  
29 forcing. Therefore, the EC method can be applied to constrain estimates of GPP due to one or the other, or both the effects.  
30 The models, however, document a higher radiative effect than fertilization at high CO<sub>2</sub> concentrations, i.e. 3×CO<sub>2</sub> and higher.  
31 An intriguing conclusion from our analysis is that the time-rate of forcing has an effect on GPP changes, that is, the projected  
32 GPP enhancement to CO<sub>2</sub> forcing seems to be dependent on how the forcing is applied over time, as in different scenarios or  
33 RCPs. This aspect is presently not well understood and requires further study.



1 The analyses and inferences presented in this article lead to the following concrete result. The uncertainty on EC estimate of  
2 GPP enhancement in NHL ( $\Delta\text{GPP} = +3.4 \text{ Pg C yr}^{-1}$ ) for a doubling of pre-industrial atmospheric  $\text{CO}_2$  concentration is  $\pm 0.2$   
3  $\text{Pg C yr}^{-1}$  (Winkler et al., 2018). This EC estimate is 60% larger than the conventionally used average of model projections  
4 (44% higher at the global scale), leading Winkler et al. (2018) to conclude that most CMIP5 models included in their analysis  
5 were largely underestimating photosynthetic production.

6 In this article, we scrutinized potential sources of uncertainty and limitations of the applicability of the EC method. Our  
7 findings are illustrated by means of a case study in carbon cycle research, however, are generally relevant and applicable in  
8 Earth system sciences.





- 1 *Author contributions.* All authors contributed ideas and to writing of the manuscript. A.J.W. did the analysis.
  
- 2 *Competing interests.* The authors declare that they have no conflict of interest.
  
- 3 *Acknowledgements.* We thankfully acknowledge T. Park and C. Chen for their help with remote sensing data. We thank G. Lasslop for
- 4 reviewing the manuscript. R.B.M. thanks Alexander von Humboldt Foundation and NASA's Earth Science Division for funding support that
- 5 made his participation possible in this research.



## 1 References

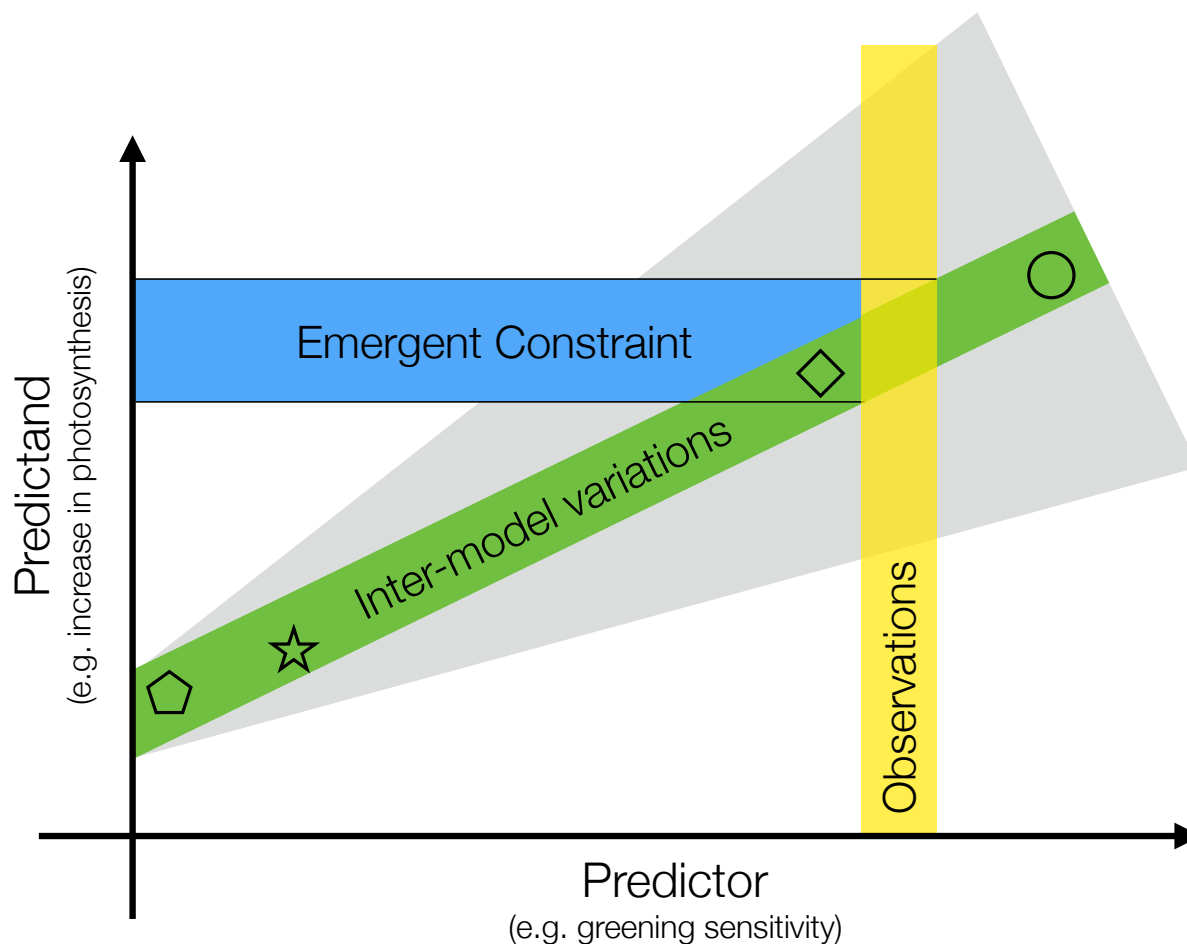
- 2 Anav, A., Friedlingstein, P., Kidston, M., Bopp, L., Ciais, P., Cox, P., Jones, C., Jung, M., Myneni, R., and Zhu, Z.: Evaluating the Land and  
3 Ocean Components of the Global Carbon Cycle in the CMIP5 Earth System Models, *J. Climate*, 26, 6801–6843, 2013.
- 4 Anav, A., Friedlingstein, P., Beer, C., Ciais, P., Harper, A., Jones, C., Murray-Tortarolo, G., Papale, D., Parazoo, N. C., Peylin, P., Piao, S.,  
5 Sitch, S., Viovy, N., Wiltshire, A., and Zhao, M.: Spatiotemporal patterns of terrestrial gross primary production: A review, *Rev. Geophys.*,  
6 53, 2015RG000 483, 2015.
- 7 Arora, V. K., Scinocca, J. F., Boer, G. J., Christian, J. R., Denman, K. L., Flato, G. M., Kharin, V. V., Lee, W. G., and Merryfield, W. J.:  
8 Carbon emission limits required to satisfy future representative concentration pathways of greenhouse gases, *Geophys. Res. Lett.*, 38,  
9 L05 805, 2011.
- 10 Arora, V. K., Boer, G. J., Friedlingstein, P., Eby, M., Jones, C. D., Christian, J. R., Bonan, G., Bopp, L., Brovkin, V., Cadule, P., Hajima, T.,  
11 Ilyina, T., Lindsay, K., Tjiputra, J. F., and Wu, T.: Carbon–Concentration and Carbon–Climate Feedbacks in CMIP5 Earth System Models,  
12 *J. Climate*, 26, 5289–5314, 2013.
- 13 Boé, J., Hall, A., and Qu, X.: September sea-ice cover in the Arctic Ocean projected to vanish by 2100, *Nature Geoscience*, 2, 341–343,  
14 2009.
- 15 Bracegirdle, T. J. and Stephenson, D. B.: Higher precision estimates of regional polar warming by ensemble regression of climate model  
16 projections, *Clim Dyn*, 39, 2805–2821, 2012a.
- 17 Bracegirdle, T. J. and Stephenson, D. B.: On the Robustness of Emergent Constraints Used in Multimodel Climate Change Projections of  
18 Arctic Warming, *J. Climate*, 26, 669–678, 2012b.
- 19 Cook, B. I. and Pau, S.: A Global Assessment of Long-Term Greening and Browning Trends in Pasture Lands Using the GIMMS LAI3g  
20 Dataset, *Remote Sensing*, 5, 2492–2512, 2013.
- 21 Cox, P. M., Pearson, D., Booth, B. B., Friedlingstein, P., Huntingford, C., Jones, C. D., and Luke, C. M.: Sensitivity of tropical carbon to  
22 climate change constrained by carbon dioxide variability, *Nature*, 494, 341–344, 2013.
- 23 Cox, P. M., Huntingford, C., and Williamson, M. S.: Emergent constraint on equilibrium climate sensitivity from global temperature vari-  
24 ability, *Nature*, 553, 319–322, 2018.
- 25 Eyring, V., Bony, S., Meehl, G. A., Senior, C. A., Stevens, B., Stouffer, R. J., and Taylor, K. E.: Overview of the Coupled Model Intercom-  
26 parison Project Phase 6 (CMIP6) experimental design and organization, *Geosci. Model Dev.*, 9, 1937–1958, 2016.
- 27 Flato, G., Marotzke, J., Abiodun, B., Braconnot, P., Chou, S., Collins, W., Cox, P., Driouech, F., Emori, S., Eyring, V., Forest, C., Gleckler,  
28 P., Guilyardi, E., Jakob, C., Kattsov, V., Reason, C., and Rummukainen, M.: Evaluation of Climate Models, in: *Climate Change 2013:*  
29 *The Physical Science Basis. Contribution of Working Group I to the Fifth Assessment Report of the Intergovernmental Panel on Climate*  
30 *Change*, edited by Stocker, T., Qin, D., Plattner, G.-K., Tignor, M., Allen, S., Boschung, J., Nauels, A., Xia, Y., Bex, V., and Midgley, P.,  
31 pp. 741–866, Cambridge University Press, Cambridge, United Kingdom and New York, NY, USA, 2013.
- 32 Forkel, M., Carvalhais, N., Rödenbeck, C., Keeling, R., Heimann, M., Thonicke, K., Zaehle, S., and Reichstein, M.: Enhanced seasonal CO<sub>2</sub>  
33 exchange caused by amplified plant productivity in northern ecosystems, *Science*, 351, 696–699, 2016.
- 34 Goetz, S. J., Bunn, A. G., Fiske, G. J., and Houghton, R. A.: Satellite-observed photosynthetic trends across boreal North America associated  
35 with climate and fire disturbance, *PNAS*, 102, 13 521–13 525, 2005.
- 36 Goll, D. S., Winkler, A. J., Raddatz, T., Dong, N., Prentice, I. C., Ciais, P., and Brovkin, V.: Carbon–nitrogen interactions in idealized  
37 simulations with JSBACH (version 3.10), *Geosci. Model Dev.*, 10, 2009–2030, 2017.



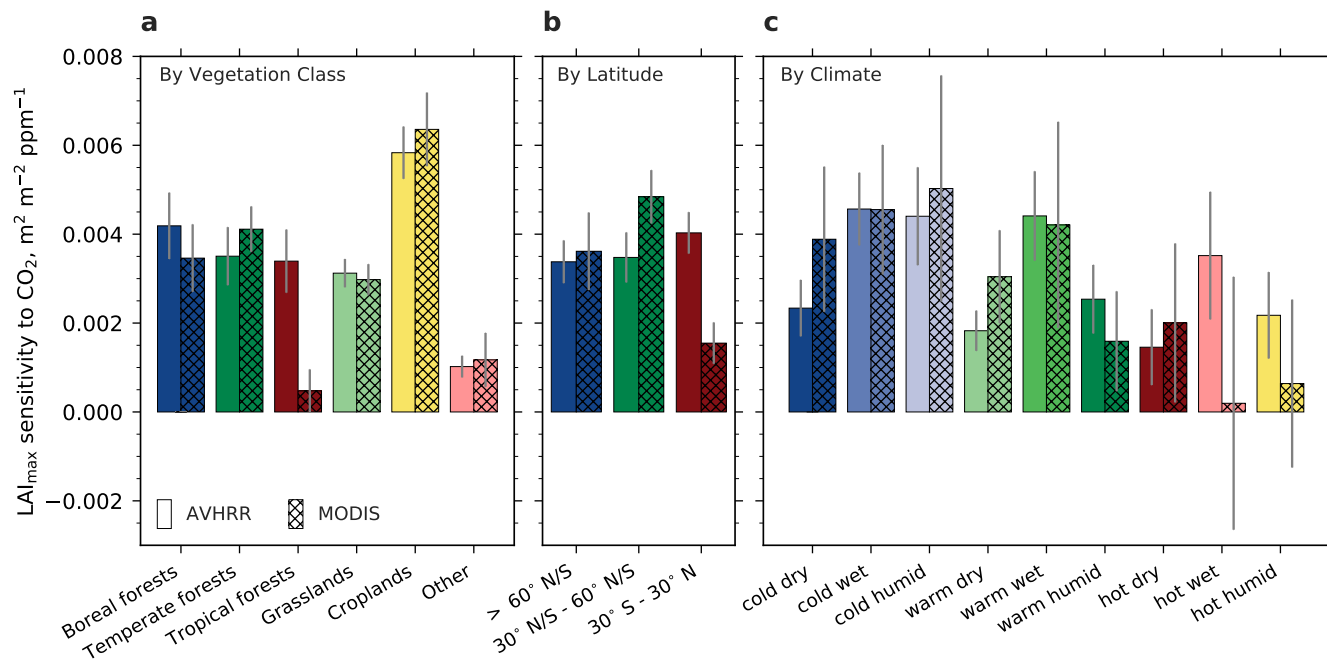
- 1 Hall, A. and Qu, X.: Using the current seasonal cycle to constrain snow albedo feedback in future climate change, *Geophys. Res. Lett.*, 33,  
2 L03 502, 2006.
- 3 Harris, I., Jones, P. D., Osborn, T. J., and Lister, D. H.: Updated high-resolution grids of monthly climatic observations – the CRU TS3.10  
4 Dataset, *International Journal of Climatology*, 34, 623–642, 2013.
- 5 Keenan, T. F., Prentice, I. C., Canadell, J. G., Williams, C. A., Wang, H., Raupach, M., and Collatz, G. J.: Recent pause in the growth rate of  
6 atmospheric CO<sub>2</sub> due to enhanced terrestrial carbon uptake, *Nature Communications*, 7, 13 428, 2016.
- 7 Klein, S. A. and Hall, A.: Emergent Constraints for Cloud Feedbacks, *Curr Clim Change Rep*, 1, 276–287, 2015.
- 8 Knutti, R.: The end of model democracy?, *Climatic Change*, 102, 395–404, 2010.
- 9 Knutti, R., Sedláček, J., Sanderson, B. M., Lorenz, R., Fischer, E. M., and Eyring, V.: A climate model projection weighting scheme account-  
10 ing for performance and interdependence, *Geophys. Res. Lett.*, 44, 1909–1918, 2017.
- 11 Kwiatkowski, L., Bopp, L., Aumont, O., Ciais, P., Cox, P. M., Laufkötter, C., Li, Y., and Séférian, R.: Emergent constraints on projections of  
12 declining primary production in the tropical oceans, *Nature Climate Change*, 7, 355–358, 2017.
- 13 Leakey, A. D. B., Ainsworth, E. A., Bernacchi, C. J., Rogers, A., Long, S. P., and Ort, D. R.: Elevated CO<sub>2</sub> effects on plant carbon, nitrogen,  
14 and water relations: six important lessons from FACE, *J Exp Bot*, 60, 2859–2876, 2009.
- 15 Lian, X., Piao, S., Huntingford, C., Li, Y., Zeng, Z., Wang, X., Ciais, P., McVicar, T. R., Peng, S., Ottlé, C., Yang, H., Yang, Y., Zhang, Y.,  
16 and Wang, T.: Partitioning global land evapotranspiration using CMIP5 models constrained by observations, *Nature Climate Change*, 8,  
17 640–646, 2018.
- 18 Mahowald, N., Lo, F., Zheng, Y., Harrison, L., Funk, C., Lombardozzi, D., and Goodale, C.: Projections of leaf area index in earth system  
19 models, *Earth Syst. Dynam.*, 7, 211–229, 2016.
- 20 Mao, J., Ribes, A., Yan, B., Shi, X., Thornton, P. E., Séférian, R., Ciais, P., Myneni, R. B., Douville, H., Piao, S., Zhu, Z., Dickinson,  
21 R. E., Dai, Y., Ricciuto, D. M., Jin, M., Hoffman, F. M., Wang, B., Huang, M., and Lian, X.: Human-induced greening of the northern  
22 extratropical land surface, *Nature Clim. Change*, 6, 959–963, 2016.
- 23 Myneni, R., Keeling, C. D., Tucker, C. J., Asrar, G., and Nemani, R. R.: Increased plant growth in the northern high latitudes from 1981 to  
24 1991, *Nature*, 386, 698–702, 1997.
- 25 Myneni, R. B., Hoffman, S., Knyazikhin, Y., Privette, J. L., Glassy, J., Tian, Y., Wang, Y., Song, X., Zhang, Y., Smith, G. R., Lotsch, A.,  
26 Friedl, M., Morisette, J. T., Votava, P., Nemani, R. R., and Running, S. W.: Global products of vegetation leaf area and fraction absorbed  
27 PAR from year one of MODIS data, *Remote Sensing of Environment*, 83, 214–231, 2002.
- 28 Nemani, R. R., Keeling, C. D., Hashimoto, H., Jolly, W. M., Piper, S. C., Tucker, C. J., Myneni, R. B., and Running, S. W.: Climate-Driven  
29 Increases in Global Terrestrial Net Primary Production from 1982 to 1999, *Science*, 300, 1560–1563, 2003.
- 30 Olson, D. M., Dinerstein, E., Wikramanayake, E. D., Burgess, N. D., Powell, G. V. N., Underwood, E. C., D’amico, J. A., Itoua, I., Strand,  
31 H. E., Morrison, J. C., Loucks, C. J., Allnut, T. F., Ricketts, T. H., Kura, Y., Lamoreux, J. F., Wettengel, W. W., Hedao, P., and Kassem,  
32 K. R.: Terrestrial Ecoregions of the World: A New Map of Life on Earth, *BioScience*, 51, 933–938, 2001.
- 33 Park, T., Ganguly, S., Tømmervik, H., Euskirchen, E. S., Høgda, K.-A., Karlsen, S. R., Brovkin, V., Nemani, R. R., and Myneni, R. B.:  
34 Changes in growing season duration and productivity of northern vegetation inferred from long-term remote sensing data, *Environ. Res.*  
35 *Lett.*, 11, 084 001, 2016.
- 36 Piao, S., Nan, H., Huntingford, C., Ciais, P., Friedlingstein, P., Sitch, S., Peng, S., Ahlström, A., Canadell, J. G., Cong, N., Levis, S., Levy,  
37 P. E., Liu, L., Lomas, M. R., Mao, J., Myneni, R. B., Peylin, P., Poulter, B., Shi, X., Yin, G., Viovy, N., Wang, T., Wang, X., Zaehle,



- 1 S., Zeng, N., Zeng, Z., and Chen, A.: Evidence for a weakening relationship between interannual temperature variability and northern  
2 vegetation activity, *Nature Communications*, 5, 5018, 2014.
- 3 Pinzon, J. E. and Tucker, C. J.: A Non-Stationary 1981–2012 AVHRR NDVI3g Time Series, *Remote Sensing*, 6, 6929–6960, 2014.
- 4 Poulter, B., Frank, D., Ciais, P., Myneni, R. B., Andela, N., Bi, J., Broquet, G., Canadell, J. G., Chevallier, F., Liu, Y. Y., Running, S. W.,  
5 Sitch, S., and van der Werf, G. R.: Contribution of semi-arid ecosystems to interannual variability of the global carbon cycle, *Nature*, 509,  
6 600–603, 2014.
- 7 Qu, X. and Hall, A.: On the persistent spread in snow-albedo feedback, *Clim Dyn*, 42, 69–81, 2014.
- 8 Sherwood, S. C., Bony, S., and Dufresne, J.-L.: Spread in model climate sensitivity traced to atmospheric convective mixing, *Nature*, 505,  
9 37–42, 2014.
- 10 Stephenson, D. B., Collins, M., Rougier, J. C., and Chandler, R. E.: Statistical problems in the probabilistic prediction of climate change,  
11 *Environmetrics*, 23, 364–372, 2012.
- 12 Taylor, K. E., Stouffer, R. J., and Meehl, G. A.: A summary of the CMIP5 experiment design, *PCDMI Rep.*, p. 33, 2009.
- 13 Taylor, K. E., Stouffer, R. J., and Meehl, G. A.: An Overview of Cmpip5 and the Experiment Design, *BAMS*, 93, 485–498, 2012.
- 14 Vuuren, D. P. v., Edmonds, J., Kainuma, M., Riahi, K., Thomson, A., Hibbard, K., Hurtt, G. C., Kram, T., Krey, V., Lamarque, J.-F., Masui,  
15 T., Meinshausen, M., Nakicenovic, N., Smith, S. J., and Rose, S. K.: The representative concentration pathways: an overview, *Climatic  
16 Change*, 109, 5–31, 2011.
- 17 Wang, J., Zeng, N., Liu, Y., and Bao, Q.: To what extent can interannual CO<sub>2</sub> variability constrain carbon cycle sensitivity to climate change  
18 in CMIP5 Earth System Models?, *Geophys. Res. Lett.*, 41, 3535–3544, 2014.
- 19 Wenzel, S., Cox, P. M., Eyring, V., and Friedlingstein, P.: Emergent constraints on climate-carbon cycle feedbacks in the CMIP5 Earth system  
20 models, *J. Geophys. Res. Biogeosci.*, 119, 794–807, 2014.
- 21 Wenzel, S., Eyring, V., Gerber, E. P., and Karpechko, A. Y.: Constraining Future Summer Austral Jet Stream Positions in the CMIP5 Ensemble  
22 by Process-Oriented Multiple Diagnostic Regression, *J. Climate*, 29, 673–687, 2015.
- 23 Wenzel, S., Cox, P. M., Eyring, V., and Friedlingstein, P.: Projected land photosynthesis constrained by changes in the seasonal cycle of  
24 atmospheric CO<sub>2</sub>, *Nature*, 538, 499–501, 2016.
- 25 Winkler, A. J., Myneni, R. B., Alexandrov, G., and Brovkin, V.: Earth System Models Underestimate Carbon Fixation by Plants in the High  
26 Latitudes, *Nature Communications*, in revision, 2018.
- 27 Yan, K., Park, T., Yan, G., Chen, C., Yang, B., Liu, Z., Nemani, R. R., Knyazikhin, Y., and Myneni, R. B.: Evaluation of MODIS LAI/FPAR  
28 Product Collection 6. Part 1: Consistency and Improvements, *Remote Sensing*, 8, 359, 2016a.
- 29 Yan, K., Park, T., Yan, G., Liu, Z., Yang, B., Chen, C., Nemani, R. R., Knyazikhin, Y., and Myneni, R. B.: Evaluation of MODIS LAI/FPAR  
30 Product Collection 6. Part 2: Validation and Intercomparison, *Remote Sensing*, 8, 460, 2016b.
- 31 Zhu, Z., Bi, J., Pan, Y., Ganguly, S., Anav, A., Xu, L., Samanta, A., Piao, S., Nemani, R. R., and Myneni, R. B.: Global Data Sets of Vegetation  
32 Leaf Area Index (LAI)3g and Fraction of Photosynthetically Active Radiation (FPAR)3g Derived from Global Inventory Modeling and  
33 Mapping Studies (GIMMS) Normalized Difference Vegetation Index (NDVI3g) for the Period 1981 to 2011, *Remote Sensing*, 5, 927–948,  
34 2013.
- 35 Zhu, Z., Piao, S., Myneni, R. B., Huang, M., Zeng, Z., Canadell, J. G., Ciais, P., Sitch, S., Friedlingstein, P., Arneeth, A., Cao, C., Cheng, L.,  
36 Kato, E., Koven, C., Li, Y., Lian, X., Liu, Y., Liu, R., Mao, J., Pan, Y., Peng, S., Peñuelas, J., Poulter, B., Pugh, T. A. M., Stocker, B. D.,  
37 Viogy, N., Wang, X., Wang, Y., Xiao, Z., Yang, H., Zaehle, S., and Zeng, N.: Greening of the Earth and its drivers, *Nature Clim. Change*,  
38 6, 791–795, 2016.

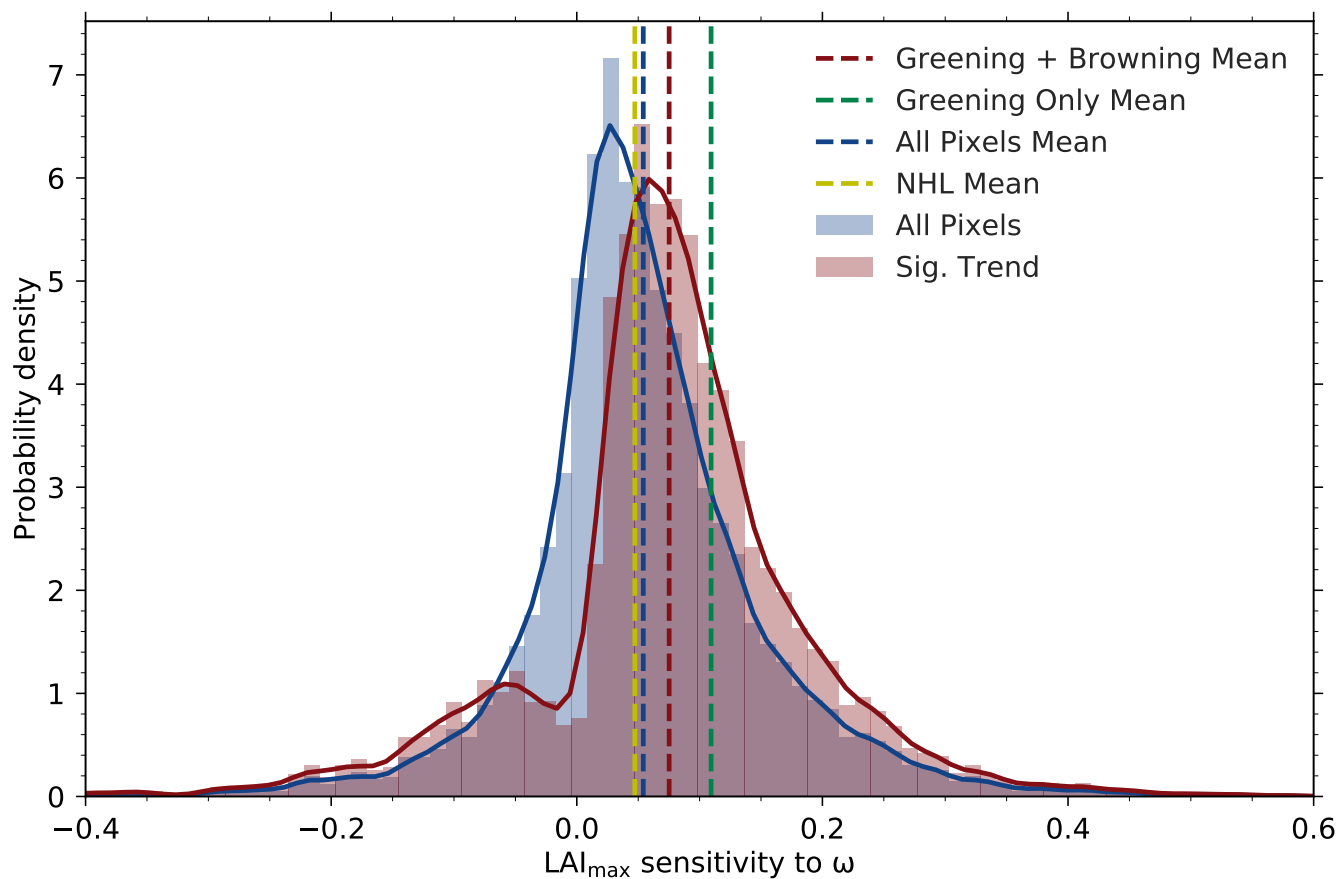


1  
 2 **Figure 1.** Schematic depiction of the Emergent Constraint (EC) method and factors affecting the uncertainty of the constrained estimate.  
 3 The predictor ( $x$  axis) is change in annual maximum of green leaf area index ( $LAI_{max}$ ) due to unit forcing ( $CO_2$  increase and associated  
 4 climatic changes) during a representative historical period. It is termed greening sensitivity in this study. The predictand ( $y$  axis) is projected  
 5 changes in Gross Primary Productivity (GPP) in response to rising  $CO_2$  concentration (e.g. for a doubling of the pre-industrial level). Both  
 6 the predictor and predictand refer to large area values, in this case, the entire Northern High Latitudes (NHL). Inter-model variations (each  
 7 symbol represents a model) in matching pairs of predictor and predictand result in a linear relationship between the two (green band), i.e. the  
 8 ratio (predictand/predictor) is approximately constant across the model ensemble. The slope depends on forcing attributes (gray shading),  
 9 such as its level ( $CO_2$  concentration, Sect. 3.4), time rate of application (scenarios such as various RCPs, Sect. 3.4) and different effects  
 10 (i.e. fertilization, radiative, etc., Sect. 3.5). The observed sensitivity (yellow vertical bar) is used to find the constrained estimate of the  
 11 predictand (i.e. change in GPP). The ability to accurately estimate the predictor depends on the source of observational data (Sect. 3.1), and  
 12 its spatial (Sect. 3.2) and temporal variability (Sect. 3.3). Observed (yellow bar) and modeled predictor values ( $x$  coordinate of symbols) must  
 13 be obtained from matching time periods, i.e. at the same level of historical forcing, to ensure comparability (Sect. 3.4). All these factors,  
 14 together with the goodness-of-fit of inter-model variations (width of green shading), finally define the uncertainty of the derived constrained  
 15 estimate (blue horizontal bar with black solid lines depicting the upper and lower bound of uncertainty).



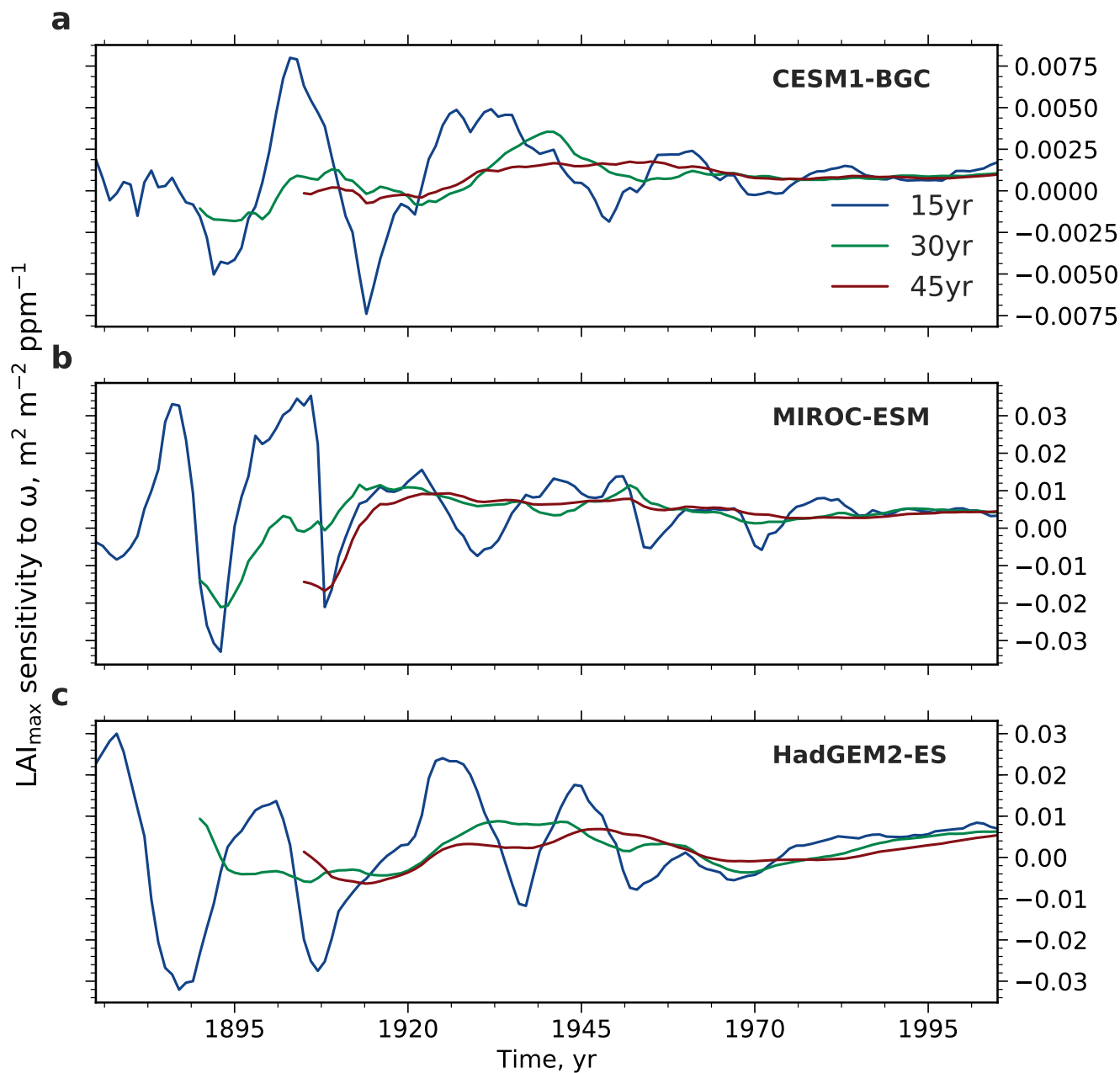
1  
2

3 **Figure 2.** Bar charts showing regression slopes of  $LAI_{max}$  against atmospheric  $CO_2$  concentration for broad vegetation classes (a, Olson  
 4 et al. (2001), latitudinal bands (b) and climate regimes (c). The class "Other" includes deserts, mangroves, barren and urban land, snow  
 5 and ice, and permanent wetlands. The climatic boundaries are defined as follows - cold:  $< 10^\circ C$ ; warm:  $> 10^\circ C$  &  $< 25^\circ C$ ; hot:  $> 25^\circ$   
 6  $C$ ; dry:  $< 500 \text{ mm a}^{-1}$ ; wet:  $> 500 \text{ mm a}^{-1}$  &  $< 1000 \text{ mm a}^{-1}$ ; humid:  $> 1000 \text{ mm a}^{-1}$ . Sensitivities evaluated from data from two  
 7 satellite-borne sensors are shown, AVHRR (1982 – 2016, Pinzon and Tucker (2014)) and MODIS (2000 – 2016, Yan et al. (2016a, b)). Grey  
 8 bars indicate the standard error of the best linear fit.



1  
2

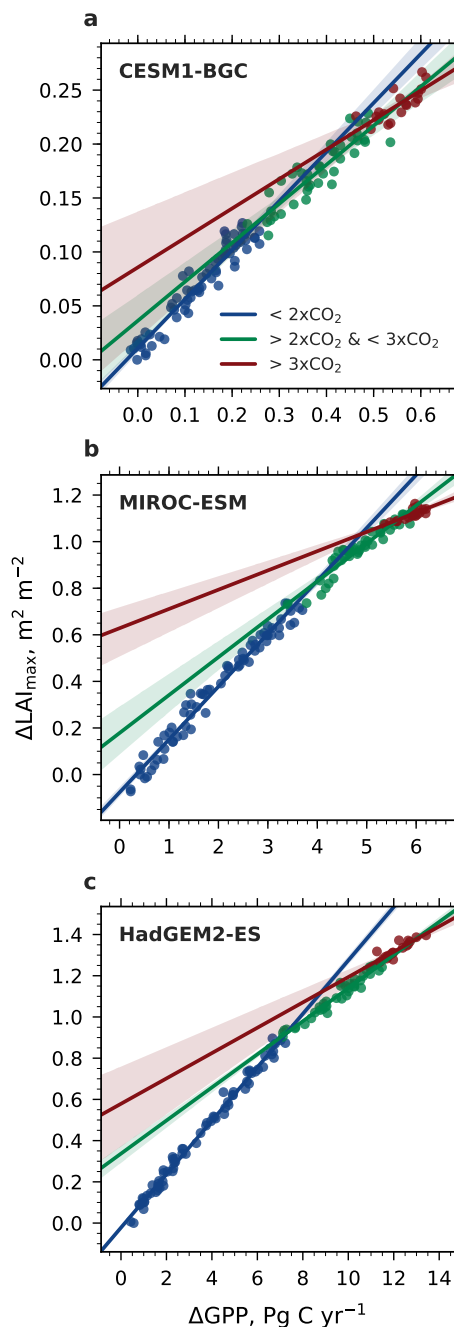
3 **Figure 3.** Histograms and associated probability density functions (Gaussian kernel density estimation) of observed  $LAI_{max}$  sensitivity to  
4  $\omega$  at pixel scale for the northern high latitudinal band ( $> 60^\circ$  N, data from AVHRR sensor). Blue color depicts the distribution of  $LAI_{max}$   
5 sensitivities of all pixels and the red color for pixels with statistically significant (Mann-Kendall test,  $p < 0.1$ ) greening or browning trends  
6 (the dashed lines denote the respective mean value). The green dashed line shows the mean value of 'greening' pixels only, whereas the  
7 yellow dashed line shows the  $LAI_{max}$  sensitivity to  $\omega$  for the entire northern high latitudinal belt.



1  
2

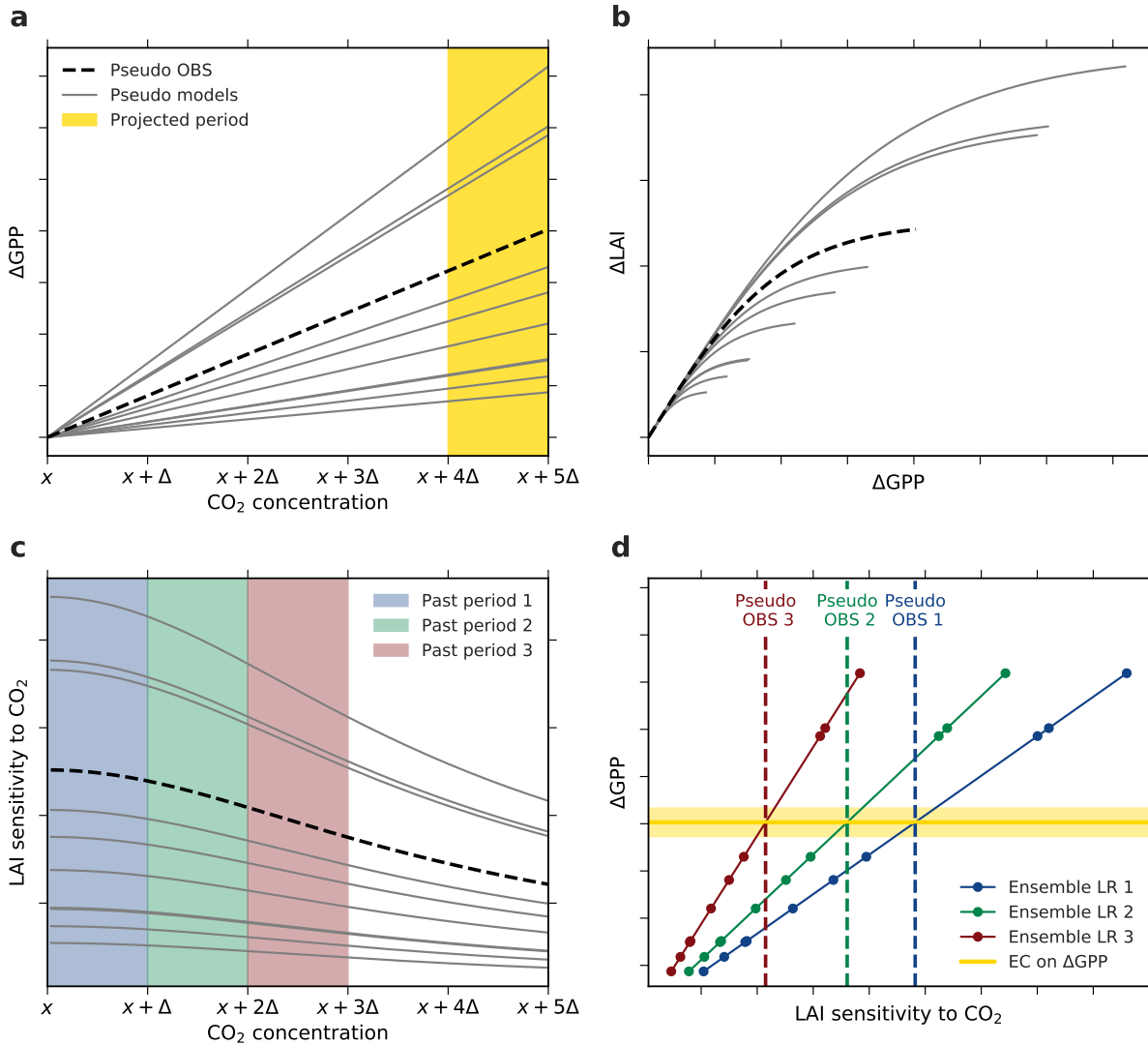
3 **Figure 4.** Temporal variation of LAI<sub>max</sub> sensitivity to  $\omega$  in three selected CMIP5 models spanning the full range from low (CESM1-BGC,  
4 a), to closest-to-observations (MIROC-ESM, b), to high-end (HadGEM2-ES, c). The colored lines show LAI<sub>max</sub> sensitivity variations for  
5 moving windows of varying length of 15 (blue), 30 (green), and 45 (red) years over the historical period from 1860 to 2005.





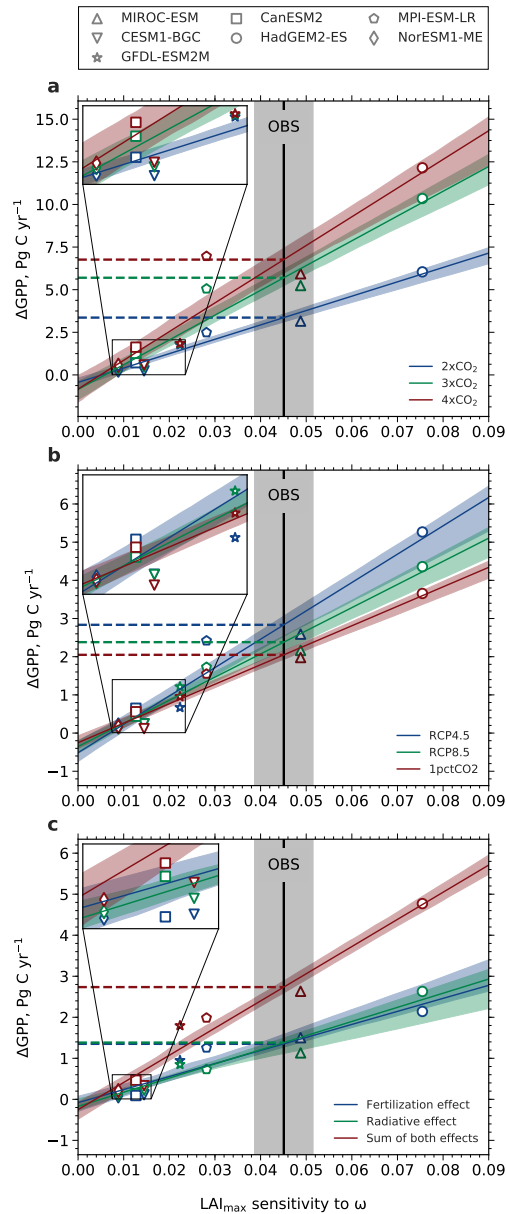
1

2 **Figure 5.** Correlation of  $\Delta LAI_{max}$  and  $\Delta GPP$  with increasing CO<sub>2</sub> forcing, starting from a pre-industrial concentration of 280 ppm (1xCO<sub>2</sub>)  
3 to 4xCO<sub>2</sub> (CMIP5 1pctCO2 simulations). Results are shown for three selected CMIP5 models spanning the full range of LAI<sub>max</sub> sensitivity  
4 to  $\omega$ , low-end: CESM1-BGC (a), closest-to-observations: MIROC-ESM (b), and high-end: HadGEM2-ES (c). Blue colored dots show the  
5 relation between 1xCO<sub>2</sub> and 2xCO<sub>2</sub>, green colored dots between 2xCO<sub>2</sub> and 3xCO<sub>2</sub>, and red colored dots between 3xCO<sub>2</sub> and 4xCO<sub>2</sub>.  
6 The respective colored lines represent the best linear fit through those dots and the shading represents the 95% confidence interval.



1

2 **Figure 6.** Gedankenexperiment to examine the applicability of Emergent Constraints analysis under the assumption of an idealized linear /  
 3 nonlinear behavior of the system (Case 3, Table A1). **a**, Changes in GPP relate linearly to changes in  $CO_2$  concentration. The yellow band  
 4 marks the projection period of interest, i.e. the period of  $CO_2$  concentration from  $x + 4\Delta$  to  $x + 5\Delta$ . **b**, The increment in LAI with  
 5 increasing GPP is assumed to decrease with rising  $CO_2$  concentration (described by a hyperbolic tangent function). The parameterization in  
 6 the linear and nonlinear functions for pseudo observations (dashed black line) as well as models (solid grey lines) are determined randomly  
 7 for each model. **c**, The diagnostic variable, LAI sensitivity to  $CO_2$ , is decreasing with increasing  $CO_2$  as a consequence of the nonlinear  
 8 relation between  $\Delta GPP$  and  $\Delta LAI$ . The colored bands indicate three 'past' periods from  $x$  to  $x + \Delta$  (blue),  $x + \Delta$  to  $x + 2\Delta$  (green),  
 9 and  $x + 2\Delta$  to  $x + 3\Delta$  (red). **d**, Linear relationships among the pseudo model ensembles (Ensemble LR, colored lines) between LAI  
 10 sensitivities to  $CO_2$  of the three past periods and  $\Delta GPP$  from the projected period. Colored dots mark different models and the dashed lines  
 11 represent associated pseudo observations for the respective historical period. Yellow solid line depicts the constant Emergent Constraint on  
 12 projected  $\Delta GPP$  irrespective of the past period.



1

2 **Figure 7.** Linear relationships between historical sensitivity of  $LAI_{max}$  to  $\omega$  and absolute increase of GPP at different levels (a), different  
 3 time-rates (b) as well as effects of rising  $CO_2$  (c). The black solid line depicts the observational sensitivity including the standard error (grey  
 4 shading). Each CMIP5 model is represented by a distinct marker (legend at the top). The colored lines show the best linear fits including the  
 5 68% confidence interval estimated by bootstrapping across the model ensemble. The colored dashed lines indicate the derived constraints on  
 6  $\Delta GPP$ . a, Absolute changes in GPP at different levels of  $CO_2$ :  $2 \times CO_2$  (blue),  $3 \times CO_2$  (green), and  $4 \times CO_2$  (red). b, Absolute changes in  
 7 GPP for rising  $CO_2$  concentration from 380 to 535 ppm at different time-rates: RCP4.5 (90 yr, blue), RCP8.5 (45 yr, green), and 1pctCO2  
 8 (30 yr, red). c, Absolute changes in GPP due to the two disentangled effects of  $CO_2$  at  $2 \times CO_2$  in idealized simulations: Fertilization effect  
 9 (esmFixClim1, blue), radiative effect (esmFdbk1, green), and the sum of both effects (red).



- 1 **Table 1.** Coefficients of determination ( $R^2$ ) of LAI<sub>max</sub> sensitivity to CO<sub>2</sub> for different large-scale aggregated regions. Data are from two  
 2 optical remote sensors of different time length, AVHRR (1982 – 2016) and MODIS (2000 – 2016). Asterisks denote non-significant values:  
 3 \*\* p > 0.1; \* p > 0.05.

Correlation coefficient $R^2$	AVHRR	MODIS
<b>Biomes</b>		
Boreal forests	0.49	0.58
Temperate forests	0.47	0.81
Tropical forests	0.41	0.06**
Graslands	0.75	0.83
Croplands	0.75	0.8
Other	0.35	0.2*
<b>Latitudinal Bands</b>		
> 60° N/S	0.51	0.61
30° N/S – 60° N/S	0.67	0.83
30° S – 30° N	0.65	0.26
<b>Climate Space</b>		
cold dry	0.29	0.27
cold wet	0.49	0.4
cold humid	0.33	0.21*
warm dry	0.33	0.36
warm wet	0.37	0.18*
warm humid	0.25	0.12**
hot dry	0.08*	0.08**
hot wet	0.15	0.00**
hot humid	0.13	0.01**

4



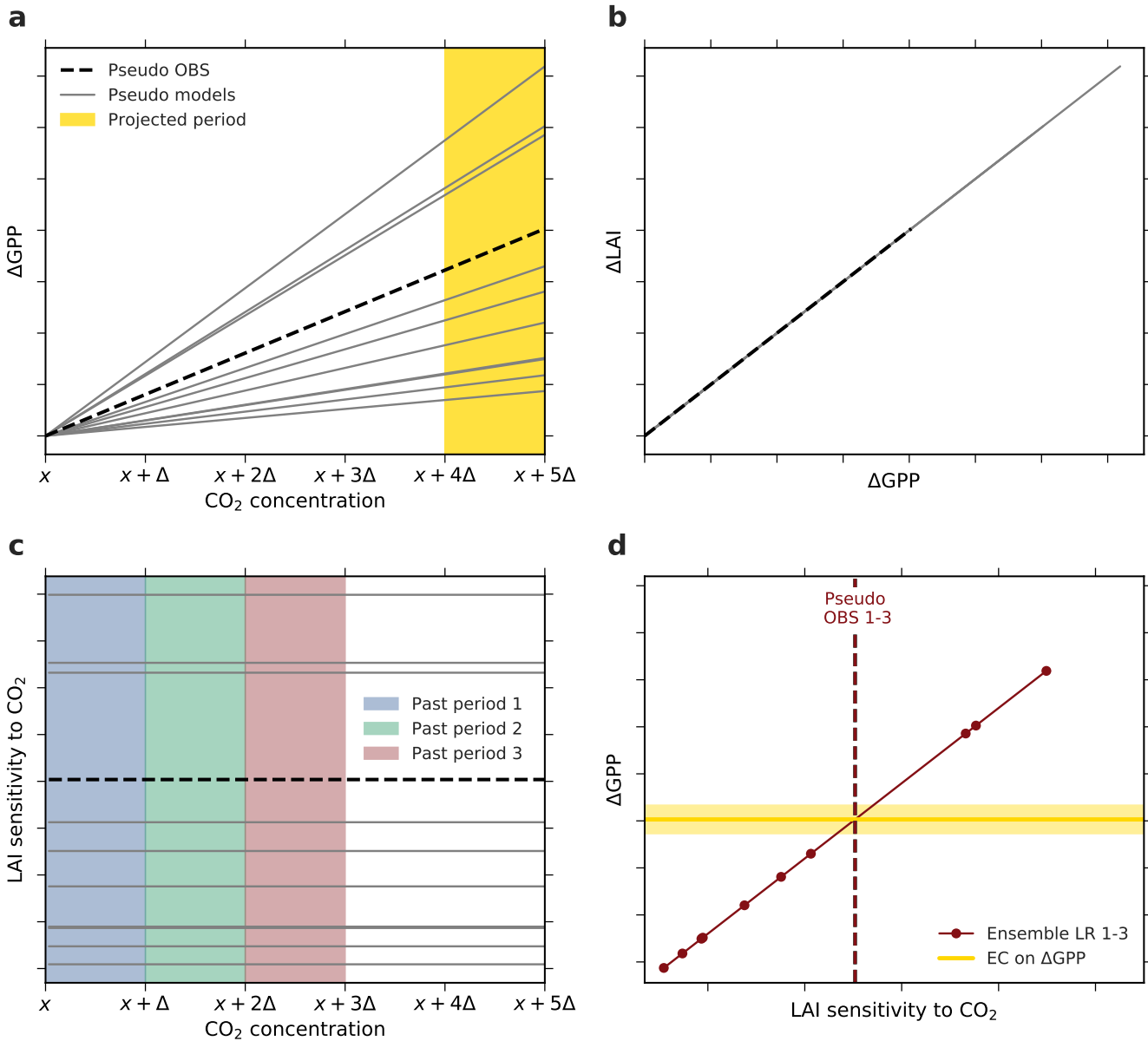
1 **Table 2.** Slopes ( $b$ ) and coefficients of determination ( $R^2$ ) for regression between changes of  $LAI_{max}$  against changes in annual mean GPP  
 2 at different atmospheric  $CO_2$  levels in all available CMIP5 models (1pctCO2 simulation). Asterisks denote non-significant values: \*\*  $p >$   
 3 0.1; \*  $p > 0.05$ .

Correlation details	< 2xCO <sub>2</sub>		> 2xCO <sub>2</sub> & < 3xCO <sub>2</sub>		> 3xCO <sub>2</sub>	
	$b$	$R^2$	$b$	$R^2$	$b$	$R^2$
MIROC-ESM	0.23	0.97	0.16	0.89	0.08	0.63
CESM1-BGC	0.45	0.93	0.36	0.82	0.27	0.62
GFDL-ESM2M	0.37	0.89	0.04	0.07**	0.01	0.12**
CanESM2	0.22	0.95	0.19	0.83	0.17	0.67
HadGEM2-ES	0.13	0.99	0.08	0.96	0.06	0.78
MPI-ESM-LR	0.13	0.94	0.09	0.78	0.04	0.51
NorESM1-ME	0.26	0.94	0.2	0.77	0.09	0.27



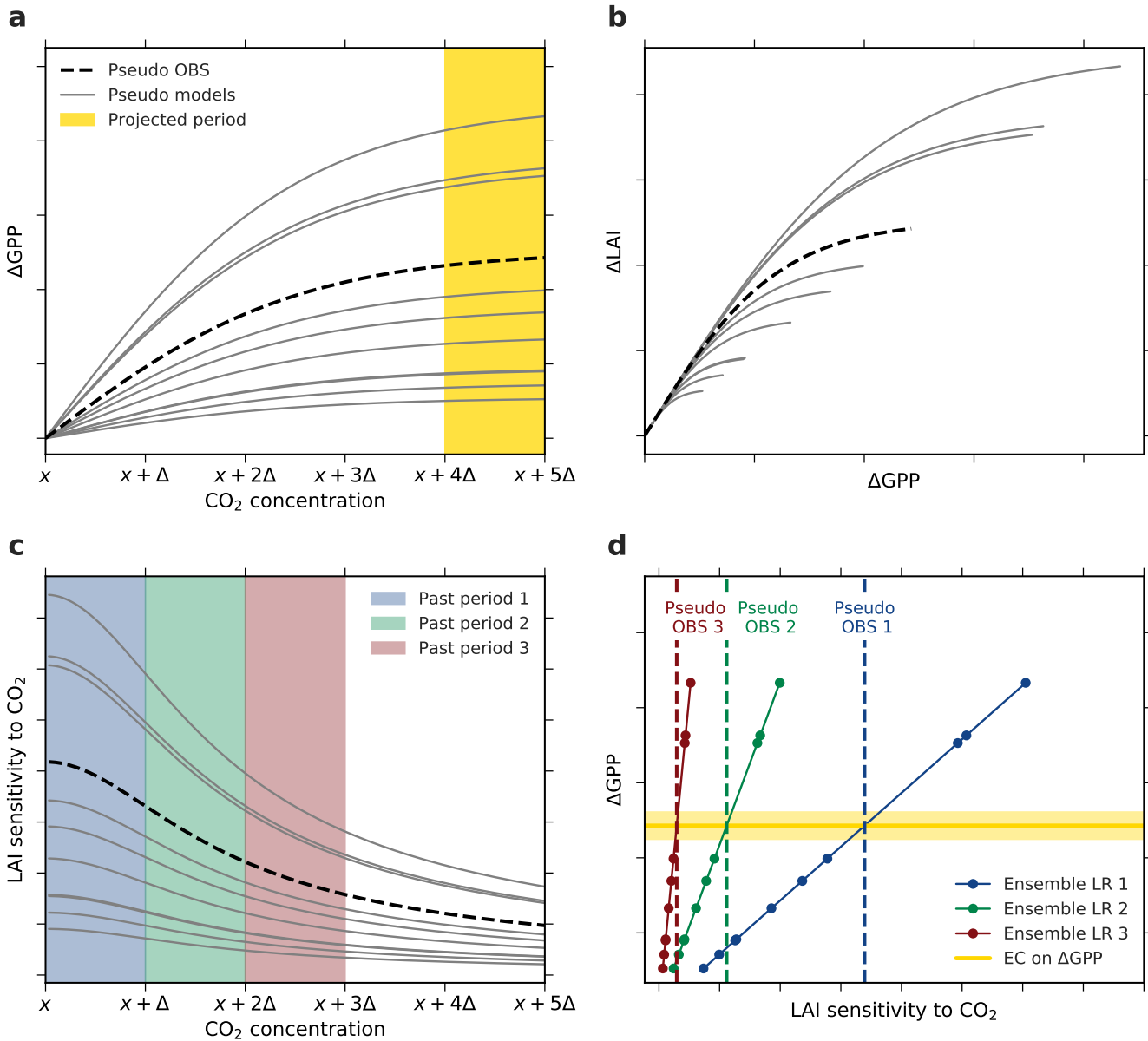
1 **Table 3.** Coefficients of determination ( $R^2$ ) of the emergent linear relationships in Figure 7 (asterisks denote non-significant values: \*\*  $p >$   
 2 0.1; \*  $p > 0.05$ ). Emergent Constraints on  $\Delta$ GPP (upper and lower bound of uncertainty in square brackets) for different atmospheric  $\text{CO}_2$   
 3 levels and fully-coupled as well as idealized setups. The rightmost column shows the increase of  $\Delta$ GPP for an increment of  $1 \times \text{CO}_2$ . The  
 4 lowermost section compares EC estimates of  $\Delta$ GPP for equivalent changes in  $\text{CO}_2$  concentration ( $\text{CO}_2$  rises from 380 to 535 ppm), but for  
 5 different time-rates.

	$R^2$	EC $\Delta$ GPP estimate ( $\text{Pg C yr}^{-1}$ )	EC $\Delta$ GPP for $\Delta 1 \times \text{CO}_2$ ( $\text{Pg C yr}^{-1}$ )
<b>2xCO<sub>2</sub></b>			
Fully coupled (1pctCO <sub>2</sub> )	0.96	3.36 [3.15, 3.56]	–
CO <sub>2</sub> fertilization only (esmFixClim1)	0.88	1.35 [1.29, 1.62]	–
Radiative effect only (esmFdbk1)	0.94	1.38 [1.13, 1.51]	–
Sum of both effects (esmFixClim1 + esmFdbk1)	0.95	2.74 [2.6, 2.9]	–
<b>3xCO<sub>2</sub></b>			
Fully coupled (1pctCO <sub>2</sub> )	0.93	5.7 [5.26, 6.16]	2.34
CO <sub>2</sub> fertilization only (esmFixClim1)	0.92	2.15 [2.02, 2.37]	0.79
Radiative effect only (esmFdbk1)	0.98	2.53 [2.3, 2.66]	1.15
6 Sum of both effects (esmFixClim1 + esmFdbk1)	0.96	4.68 [4.38, 4.97]	1.94
<b>4xCO<sub>2</sub></b>			
Fully coupled (1pctCO <sub>2</sub> )	0.88	6.76 [6.08, 7.53]	1.06
CO <sub>2</sub> fertilization only (esmFixClim1)	0.88	2.42 [2.23, 2.74]	0.28
Radiative effect only (esmFdbk1)	0.97	3.06 [2.83, 3.2]	0.53
Sum of both effects (esmFixClim1 + esmFdbk1)	0.95	5.49 [5.09, 5.85]	0.81
<b>380 – 535 ppm CO<sub>2</sub></b>			
Slow increase in CO <sub>2</sub> (RCP4.5)	0.93	2.84 [2.54, 3.08]	–
Medium-fast increase in CO <sub>2</sub> (RCP8.5)	0.96	2.38 [2.18, 2.55]	–
Rapid increase in CO <sub>2</sub> (1pctCO <sub>2</sub> )	0.96	2.05 [1.94, 2.16]	–



1  
2

3 **Figure A1.** Gedankenexperiment to examine the applicability of the Emergent Constraints analysis assuming an idealized linear / linear  
 4 behavior of the system (Case 1, Table A1). **a**, Changes in GPP relate linearly to changes in CO<sub>2</sub> concentration. The yellow band marks  
 5 the projection period of interest, i.e. the period of CO<sub>2</sub> concentration from  $x + 4\Delta$  to  $x + 5\Delta$ . **b**, Changes in LAI relate linearly to  
 6 changes in GPP. The parameterization in the linear functions for pseudo observations (dashed black line) as well as models (solid grey lines)  
 7 are determined randomly for each model. **c**, The diagnostic variable, LAI sensitivity to CO<sub>2</sub>, remains constant with increasing CO<sub>2</sub> as a  
 8 consequence of the overall linear characteristics of the system. The colored bands indicate three 'past' periods from  $x$  to  $x + \Delta$  (blue),  
 9  $x + \Delta$  to  $x + 2\Delta$  (green), and  $x + 2\Delta$  to  $x + 3\Delta$  (red). **d**, Linear relationships among the pseudo model ensembles (Ensemble LR 1-3  
 10 on top of each other, red) between LAI sensitivity to CO<sub>2</sub> of the three past periods and  $\Delta$ GPP from the projected period. Red dots mark  
 11 different models and the dashed line represents associated pseudo observations for all three historical periods. Yellow solid line depicts the  
 12 constant Emergent Constraint on projected  $\Delta$ GPP irrespective of the past period .



1  
2

3 **Figure A2.** Gedankenexperiment to examine the applicability of the Emergent Constraints analysis assuming an idealized nonlinear / non-  
 4 linear behavior of the system (Case 4, Table A1). **a**,  $\Delta GPP$  decreases with increasing  $CO_2$  concentration (described by a hyperbolic tangent  
 5 function). The yellow band marks the projected period of interest, i.e. the period of  $CO_2$  concentration from  $x + 4\Delta$  to  $x + 5\Delta$ . **b**, Also  
 6  $\Delta LAI$  decreases with increasing GPP (described by a hyperbolic tangent function). The parameterization in the hyperbolic tangent functions  
 7 for pseudo observations (dashed black line) as well as models (solid grey lines) are determined randomly for each model. **c**, The diagnostic  
 8 variable, LAI sensitivity to  $CO_2$ , is decreasing with increasing  $CO_2$  as a consequence of the overall saturating characteristics of the system.  
 9 The colored bands indicate three 'past' periods from  $x$  to  $x + \Delta$  (blue),  $x + \Delta$  to  $x + 2\Delta$  (green), and  $x + 2\Delta$  to  $x + 3\Delta$  (red). **d**, Linear  
 10 relationships among the pseudo model ensembles (Ensemble LR, colored lines) between LAI sensitivity to  $CO_2$  of the three past periods  
 11 and  $\Delta GPP$  from the projected period. Colored dots mark different models and the dashed lines represent associated pseudo observations for  
 12 respective historical period. Yellow solid line depicts the constant Emergent Constraint on projected  $\Delta GPP$  irrespective of the past period .





1 **Table A1.** Overview of four possible cases of interaction between forcing, non-observable and observable identified in the Gedankenexperi-  
 2 ment: All linear, all nonlinear, and two mixed cases.

Different assumptions	$\frac{d[\text{non-observable}]}{d[\text{forcing}]}$ , e.g. $\frac{d[\text{GPP}]}{d[\text{CO}_2]}$	$\frac{d[\text{observable}]}{d[\text{non-observable}]}$ , e.g. $\frac{d[\text{LAI}]}{d[\text{GPP}]}$
1	linear	linear
2	nonlinear	linear
3	linear	nonlinear
4	nonlinear	nonlinear

4